A&A 499, 103–119 (2009)
DOI: 10.1051/0004-6361/200810592
© ESO 2009

Astronomy & Astrophysics

Beryllium abundances and star formation in the halo and in the thick disk⋆,⋆⋆

R. Smiljanic[1,2], L. Pasquini[2], P. Bonifacio[3,4,⋆⋆⋆], D. Galli[5], R. G. Gratton[6], S. Randich[5], and B. Wolff[2]

[1] Universidade de São Paulo, IAG, Dpt. de Astronomia, Rua do Matão 1226, São Paulo-SP 05508-090, Brazil
e-mail: rodolfo@astro.iag.usp.br
[2] European Southern Observatory, Karl-Schwarzschild-Str. 2, 85748 Garching bei München, Germany
[3] GEPI, Observatoire de Paris, CNRS, Université Paris Diderot, Place Jules Janssen, 92190 Meudon, France
[4] INAF – Osservatorio Astronomico di Trieste, via G.B. Tiepolo 11, 34143 Trieste, Italy
[5] INAF – Osservatorio Astrofisico di Arcetri, Largo E. Fermi 5, 50125 Firenze, Italy
[6] INAF – Osservatorio Astronomico di Padova, Vicolo dell'Osservatorio 5, 35122 Padova, Italy

Received 14 July 2008 / Accepted 26 January 2009

ABSTRACT

Context. Beryllium is a pure product of cosmic ray spallation. This implies a relatively simple evolution in time of the beryllium abundance and suggests its use as a time-like observable.
Aims. Our goal is to derive abundances of Be in a sample of 90 stars, the largest sample of halo and thick disk stars analyzed to date. We study the evolution of Be in the early Galaxy and its dependence on kinematic and orbital parameters, and investigate its use as a cosmochronometer. Abundances of Be, Fe, and α-elements of 73 stars are employed to study the formation of the halo and the thick disk of the Galaxy.
Methods. Beryllium abundances are determined from high-resolution, high signal-to-noise UVES spectra with spectrum synthesis. Atmospheric parameters and abundances of α-elements are adopted from the literature. Lithium abundances are used to eliminate mixed stars from the sample. The properties of halo and thick disk stars are investigated in diagrams of log(Be/H) vs. [α/H], log(Be/H) vs. [Fe/H], and [α/Fe] vs. log(Be/H) and with orbital and kinematic parameters.
Results. We present our observational results in various diagrams. (i) In a log(Be/H) vs. [Fe/H] diagram we find a marginal statistical detection of a real scatter, above what is expected from measurement errors, with a larger scatter among halo stars. The detection of the scatter is further supported by the existence of pairs of stars with identical atmospheric parameters and different Be abundances; (ii) in a log(Be/H) vs. [α/Fe] diagram, the halo stars separate into two components; one is consistent with predictions of evolutionary models, while the other has too high α and Be abundances and is chemically indistinguishable from thick disk stars. This suggests that the halo is not a single uniform population where a clear age-metallicity relation can be defined; (iii) In diagrams of $R_{\rm min}$ vs. [α/Fe] and log(Be/H), the thick disk stars show a possible decrease in [α/Fe] with $R_{\rm min}$, whereas no dependence of Be with $R_{\rm min}$ is seen. This anticorrelation suggests that the star formation rate was lower in the outer regions of the thick disk, pointing towards an inside-out formation. The lack of correlation for Be indicates that it is insensitive to the local conditions of star formation.

Key words. stars: abundances – stars: late-type – Galaxy: halo – Galaxy: disk

1. Introduction

The nucleosynthetic origin of beryllium is different from most chemical elements. Beryllium is neither a product of stellar nucleosynthesis nor expected to be created by the standard homogeneous primordial nucleosynthesis in a detectable amount (Thomas et al. 1993). Its single long-lived isotope, ^{9}Be, is a pure product of cosmic-ray spallation of heavy (mostly CNO) nuclei in the interstellar medium (Reeves et al. 1970; Meneguzzi et al. 1971).

Early theoretical models of Be production in the Galaxy assumed the cosmic-ray composition to be similar to the composition of the interstellar medium (ISM). In this scenario, Be is produced by accelerated protons and α-particles colliding with CNO nuclei of the ISM (Meneguzzi & Reeves 1975; Vangioni-Flam et al. 1990; Prantzos et al. 1993), resulting in a quadratic dependence of the Be abundance with metallicity. However, observations of Be in metal-poor stars (Rebolo et al. 1988; Gilmore et al. 1992; Molaro et al. 1997a; Boesgaard et al. 1999) find a slope equal or close to one between log(Be/H) and [Fe/H], and just slightly higher for log(Be/H) and [O/H][1]. Such slopes argue that Be behaves as a primary element and its production mechanism is independent of ISM metallicity. Thus, the dominant production mechanism is now thought to be the collision of cosmic-rays composed of accelerated CNO nuclei with protons and α-particles of the ISM (Duncan et al. 1992; Cassé et al. 1995; Vangioni-Flam et al. 1998).

On the other hand, in light of some controversy about the behavior of O in metal-poor stars, Fields & Olive (1999) argue that a secondary behavior cannot be excluded. King (2001, 2002), however, reassessing data of different oxygen indicators, as well

⋆ Based on observations made with ESO VLT, at Paranal Observatory, under programs 076.B-0133 and 077.B-0507, and on data obtained from the ESO/ST-ECF Science Archive Facility and the UVES Paranal Observatory Project 266.D-5655.
⋆⋆ Tables 1–3, 6 and Appendices A–C are only available in electronic form at http://www.aanda.org
⋆⋆⋆ CIFIST Marie Curie Excellence Team

[1] [A/B] = log $[N(A)/N(B)]_\star$ – log $[N(A)/N(B)]_\odot$.

as data for other α-elements, show that a metal-poor primary mechanism is necessary to explain the observations.

As a primary element and considering cosmic-rays to be globally transported across the Galaxy, one may expect the Be abundance to be rather homogeneous at a given time in the early Galaxy. It should have a smaller scatter than the products of stellar nucleosynthesis (Suzuki et al. 1999; Suzuki & Yoshii 2001). Thus, Be would show a good correlation with time and could be employed as a cosmochronometer for the early stages of the Galaxy (Beers et al. 2000; Suzuki & Yoshii 2001).

Pasquini et al. (2004, 2007) have tested this suggestion deriving Be abundances in turn-off stars in the globular clusters NGC 6397 and NGC 6752. The Be ages derived from a model of the evolution of Be with time (Valle et al. 2002) are in excellent agreement with those derived from theoretical isochrones. Moreover, the Be abundances of these globular cluster stars are similar to the abundances of field stars with the same metallicity. These results strongly suggest that the stellar Be abundances are independent of the environment where the star was formed and support the use of Be as a cosmochronometer.

Using abundances determined by Boesgaard et al. (1999), Pasquini et al. (2005) extended the use of Be as a time scale to a sample of 20 halo and thick disk stars and investigated the evolution of the star formation rate in the early-Galaxy. Stars belonging to the two different kinematic components identified by Gratton et al. (2003a) seem to separate in a log(Be/H) vs. [O/Fe] diagram. Such separation is interpreted as indicating the formation of the two components to occur under different conditions and time scales.

Our aim in this work is to better understand the evolution of Be in the early Galaxy and its dependence on different parameters, in particular on the stellar population. We analyze an unprecedentedly large sample of halo and thick disk stars, and further investigate the use of Be as a cosmochronometer and its role as a discriminator of different stellar populations in the Galaxy. The sample and the observational data are described in Sect. 2. The details on the adopted atmospheric parameters are given in Sect. 3. The abundance determination and its uncertainties are discussed in Sect. 4 while a comparison with previous results of the literature is presented in Sect. 5. Lithium abundances are used to clean the sample from mixed stars in Sect. 6. The Galactic evolution of Be is discussed in Sect. 7, the use of Be as a chronometer is discussed in Sect. 8, while a summary is given in Sect. 9.

2. Sample selection and observational data

The sample stars were selected from the compilation by Venn et al. (2004) of several abundance and kinematic analyses of Galactic stars available in the literature. Using the available kinematic data, Venn et al. (2004) calculated the probabilities that each star belongs to the thin disk, the thick disk, or the halo. A total of 90 stars were selected for this work: 9 of them have higher probability of being thin disk stars, 30 of being thick disk stars, 49 of being halo stars; and 2 have 50% probabilities of being halo or thick disk stars. We simply assume a star belongs to a certain kinematic group when the probability of belonging to that group is higher than the probability of being in the other two groups. One of our aims is to compare stars of different populations but of similar abundances, so we tried to maximize the metallicity overlap between the two sub-samples. The halo stars range from [Fe/H] = −2.48 to −0.50 and the thick disk stars from [Fe/H] = −1.70 to −0.50, although strongly concentrated in [Fe/H] ≥ −1.00. The sample stars are listed in Table 1, together with V band magnitudes, parallaxes, absolute magnitudes, bolometric corrections, bolometric magnitudes, luminosities, and information on multiplicity. Details on these are given in the following sections.

Spectra for all stars were obtained using UVES, the *Ultraviolet and Visual Echelle Spectrograph* (Dekker et al. 2000) fed by UT2 of the VLT. UVES is a cross-dispersed echelle spectrograph able to obtain spectra from the atmospheric cut-off at 300 nm to ∼1100 nm.

For 55 stars, new spectra were obtained in service mode during two observing periods between October 2005 and September 2006. UVES was operated in dichroic mode with cross dispersers #1, #3, and #4 resulting in spectral coverage of $\lambda\lambda$300–390 nm in the blue arm and $\lambda\lambda$420–680 nm and $\lambda\lambda$660–1100 nm in the red arm, with some gaps. The spectra have a resolving power of $R \sim 35\,000$ and S/N between 25 and 150 in the Be region. The reduction was conducted with the UVES pipeline within MIDAS. While the blue arm of the spectra was always found to have enough quality for the analysis, the same was not true for the red arm that, in some cases, presented residual fringing. For them, a new reduction of the raw frames was conducted using the most recent release of the UVES Common Pipeline Library (CPL) recipes within ESORex, the ESO Recipe Execution Tool.

Reduced spectra for 4 stars were downloaded from the UVES Paranal Observatory Project (POP) Library – a library of high-resolution spectra of stars across the HR diagram (Bagnulo et al. 2003). In this library the stars were observed with both dichroic #1 and #2 covering almost all the interval between 300 and 1000 nm. The spectra have $R \sim 80\,000$ and a typical S/N ratio varying from 60 to 400 in the Be region.

For the remaining 31 stars, archive raw data in the $\lambda\lambda$300–390 nm region were retrieved from the ESO/ST-ECF science archive facility and employed in the analysis. For some stars, in particular those that do not have previous determinations of lithium abundance in the literature, raw data in the $\lambda\lambda$420–680 nm region were also retrieved. The spectra were reduced using the UVES pipeline within MIDAS and ESORex. The resolving power of these spectra varies between 35 000 and 50 000 and the S/N ratio varies between 45 and 170 in the Be region. The log book of the observations is given in Table 2 in the Appendix.

3. Atmospheric parameters

3.1. Source of the parameters

All the selected stars have been targets of previous abundance analyses. In this work, we decided to adopt the atmospheric parameters, effective temperature ($T_{\rm eff}$), surface gravity (log g), microturbulence velocity (ξ), and metallicity ([Fe/H]), determined by previous works. The adopted parameters are given in Table 3. We adopted as main reference the same high-resolution analyses quoted in the compilation by Venn et al. (2004). Our sample contains 59 stars analyzed by Fulbright (2000, F00 hereafter), 15 by Nissen & Schuster (1997, NS97 hereafter), 7 by Edvardsson et al. (1993, Ed93 hereafter), 4 by Stephens & Boesgaard (2002, SB02 hereafter), 2 by Prochaska et al. (2000, Pr00 hereafter), 1 by Gratton & Sneden (1988, GS88 hereafter), 1 by Gratton & Sneden (1991, GS91 hereafter), and 1 by McWilliam et al. (1995, McW95 hereafter).

Even though different methods were adopted to determine the parameters, we do not expect this choice to introduce any systematic effect in our analysis. The likely effect of adopting

Table 4. Methods adopted by the reference papers cited in the text to calculate the atmospheric parameters.

Reference	Temp.	Surface gravity	Microt.	Model atm.	LTE/NLTE?
F00	Exc. Eq. of Fe I lines $\log(EW/\lambda) \leq -4.80$	Ion. Eq. Fe I and Fe II $\log(EW/\lambda) \leq -4.80$	Fe I lines	Kurucz + overshooting	LTE
SB02	Exc. Eq. of Fe I lines $\log(EW/\lambda) \leq -5.15$	Average of Ion. Eq. of Fe I/Fe II and Ti I/Ti II	Fe I lines agrees with Ed93 relation	Kurucz Castelli et al. (1997)	LTE
NS97	Exc. Eq. of Fe I lines $\log(EW/\lambda) \leq -5.15$	Ion. Eq. Fe I and Fe II	Fe I lines with $\chi \geq 4$ eV	(NEW)MARCS (Ed93)	LTE
Ed93	Strömgren photometry calib. of $(b-y)$ and β	Balmer discontinuity index, c_1	Empiric relation dependent on $T_{\rm eff}$ and $\log g$	(NEW)MARCS	LTE

atmospheric parameters with possibly different scales is an increase in the scatter of the abundances. We note that Venn et al. (2004) argue that a superficial analysis of their whole sample did not show a major inconsistency or zero point difference between the results. We refer the reader to the original papers for detailed descriptions of the methods and comparisons between the results with other literature determinations. We note, however, that all the papers claim reasonable agreement with previous determinations. Moreover, as the parameters of most of the stars analyzed here (59 out of 90) come from a single reference, F00, we expect any possible difference in the scale of the parameters to have only a minor effect on the abundances.

For the completeness of the discussion, we list some information in Table 4 on the methods adopted by each relevant[2] work as the reference for the atmospheric parameters. As is clear from Table 4, F00, NS97, and SB02 adopt very similar methods based on spectroscopy to determine the atmospheric parameters. On the other hand, the method adopted by Ed93 is completely diverse, based only on photometry. In NS97 the same model atmospheres used by Edvardsson et al. are adopted. In addition, their work is a differential one with respect to two bright stars analyzed by Ed93. They therefore obtain parameters essentially on the same scale as the ones derived by Ed93, as demonstrated by their Fig. 03, which shows excellent agreement between their $T_{\rm eff}$ with temperatures derived using $(b-y)$ calibrations.

As Be abundances are calculated from lines of the ionized species, $\log g$ is the most relevant parameter for the analysis. Our sample stars are relatively bright and nearby, so we used Hipparcos parallaxes (ESA 1997) to estimate gravities. Apart from eight stars that show a significant difference (larger than 0.28 dex), the agreement is excellent. A linear fit to the points yields a line that is statistically indistinguishable from the $x = y$ line, with a rms of 0.20 dex when all the points are considered, or of 0.14 dex when the discrepant stars are excluded. These eight stars have uncertain parallaxes $\sigma_\pi/\pi \geq 0.20$ or are binary stars.

Thus, only a comparison between the results of F00 and Ed93 is necessary to ensure the consistency between the atmospheric parameters of most of the sample stars. Such a comparison is shown below.

3.2. Comparison between Edvardsson et al. and Fulbright

The comparison between the results of F00 and Ed93 was conducted to assure the detailed understanding and proper identification of any possible systematic effect introduced in the analysis.

[2] We do not include in Table 4 details on the analyses by Gratton & Sneden (1988, 1991) and by McWilliam et al. (1995), which contribute only 1 star each, and on the one by Prochaska et al. (2000), with only 2 stars, since they will have no influence at all on a possibly larger scatter of the results.

Ten stars are shared between the two analyses. Of these, seven are included in our sample. The atmospheric parameters of all the ten stars derived by the two papers are compared in Fig. 1. The effective temperatures show excellent agreement, with a mean difference of 46 K and a maximum difference of 85 K. Although the values derived by F00 are systematically lower than the ones derived by Ed93, the difference is small, well within the uncertainties of the calculations. The difference in surface gravity is also small, with a mean of 0.11 dex and a maximum of 0.19 dex, and might be related to the different adopted temperature scales. The differences in gravity are close to the uncertainty value. Finally, the metallicity ([Fe/H]) values show a mean difference of 0.10 dex and maximum of 0.21 dex. This difference seems to be systematic, because the values of F00 are always slightly higher than the ones derived by Ed93.

The comparison shows that the differences between F00 and Ed93 are not large, but can be ascribed mostly to the uncertainties in each analysis, except for the microturbulence (Fig. 1). This shows that no strong systematic effect will be present on our abundances and argues in favor of our assumption that the scales of the different papers are indeed similar, and the use of the combined set of parameters introduces only a small and acceptable dispersion on the abundances. However, we note that the observed difference in [Fe/H] might introduce some dispersion on the data points when analyzing plots like log(Be/H) vs. [Fe/H] or [Be/Fe] vs. [Fe/H]. This point has to be kept in mind and will be recalled when discussing our results.

3.3. Uncertainties of the atmospheric parameters

In Table 5 we list the uncertainties in the atmospheric parameters as calculated by each of the four papers that contribute more than two stars to our sample.

As seen in Table 5, the adopted works claim a rather low uncertainty for their $T_{\rm eff}$ values, ranging from 40 to 100 K. As discussed before, for the ten stars in common, the mean difference between the temperatures derived by Ed93 and F00 is 46 K with maximum of 85 K. These values argue in favor of the quoted uncertainties. Nevertheless, in this case we decided to adopt a rather conservative value of 100 K as representative of the associated uncertainty. This value equals the higher of the values suggested by Ed93 and might be a good estimate of the effect of mixing the temperature scales of the different papers together. However, as we will see in the following sections the uncertainty in $T_{\rm eff}$ has little influence on the derived beryllium abundance.

For the $\log g$ values, the adopted papers claim uncertainties ranging form 0.06 to 0.35 dex. The comparison between Ed93 and F00 shows a mean difference of 0.11 dex with maximum of 0.19 dex. Moreover, the comparison with $\log g$ values estimated using parallax show an rms of 0.14 dex. In particular, this comparison seems to show that the $\log g$ values are rather well

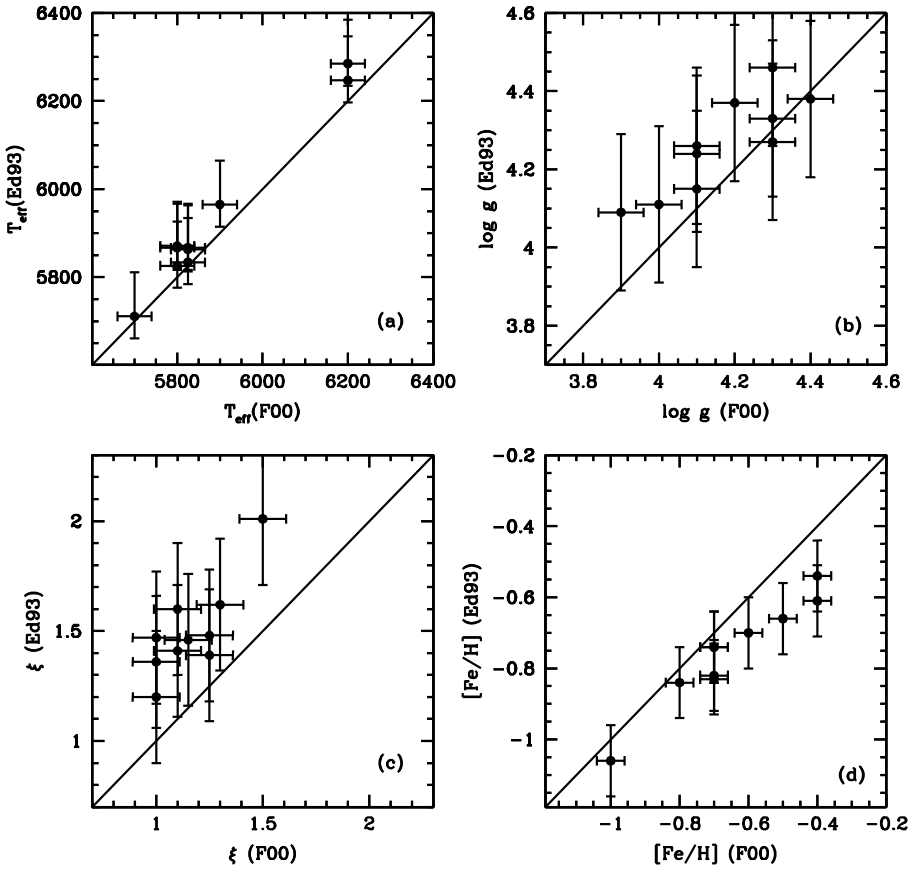

Fig. 1. Comparison of the adopted atmospheric parameters for stars shared by F00 and ED93. The error bars with the values listed in the original papers are also shown.

Table 5. Uncertainties in the adopted atmospheric parameters.

Ref.	$T_{\rm eff}$ (K)	log g	ξ (km s^{-1})	[Fe/H]
F00	±40	±0.06	±0.11	±0.04
SB02	±75	±0.35	±0.30	±0.10
NS97	±50	±0.10	–	±0.05
Ed93	$^{+100}_{-50}$	±0.20	±0.30	±0.10
adopted	±100	±0.15	±0.30	±0.15

constrained, in spite of the larger uncertainties quoted by Ed93 and SB02. Therefore, in this case we adopted a value of 0.15 dex as representative of the uncertainty in log g.

The quoted uncertainty on the microturbulence velocity (ξ) varies from 0.11 to 0.30 km s^{-1} in the adopted papers. The comparison between Ed93 and F00, however, shows larger differences with a mean of 0.31 km s^{-1} and maximum of 0.54 km s^{-1}. In this case, however, we simply decided to adopt the higher value of the quoted uncertainties, 0.30 km s^{-1}, as representative. Again, as we see below, this choice and the large differences in ξ have no significant impact on the beryllium abundances.

The adopted papers list values for the metallicity ([Fe/H]) with its uncertainty ranging from 0.04 to 0.10 dex. The comparison between Ed93 and F00, however, shows a mean difference of 0.10 dex with maximum of 0.21 dex. Mainly because of this comparison, we decided to adopt a somewhat higher value as representative of the uncertainty than the ones quoted in the adopted papers, 0.15 dex. As for the other parameters, except for log g, its influence on the final beryllium abundances is weak. The adopted uncertainty values are listed in Table 5.

4. Abundances determination

4.1. Synthetic spectra

Abundances of beryllium and, for some stars, of lithium were calculated using synthetic spectra. In this work, we adopted the codes for calculating synthetic spectrum described by Barbuy et al. (2003) and Coelho et al. (2005). We use the grids of model atmospheres calculated by the ATLAS9 program (Castelli & Kurucz 2003), without overshooting. These models assume local thermodynamic equilibrium, plane-parallel geometry, and hydrostatic equilibrium. Codes for interpolating among the grids were adopted.

On the spectra of late-type stars, only the Be II ^{2}S–^{2}P$_0$ resonance lines at 3131.065 Å and 3130.420 Å are strong enough to be useful for an abundance analysis. These lines are near the atmospheric cut-off at 3000 Å in a region of low detector sensitivity. This near-UV region is extremely crowded, full of atomic and molecular lines, some of them still lacking proper identification. The determination of Be abundances, thus, needs to be done with spectrum synthesis taking all the blending nearby features into account. Our database of molecular lines include the OH ($A^2\Sigma$-$X^2\Pi$), NH ($A^3\Pi$–$X^3\Sigma$), and CN ($B^2\Pi$–$X^2\Sigma$) band systems as implemented by Castilho et al. (1999) and the *CH* band systems ($A^2\Delta$–$X^2\Pi$), ($B^2\Sigma$–$X^2\Pi$), and ($C^2\Sigma$–$X^2\Pi$) as implemented by Meléndez et al. (2003), all of them affecting this spectral region.

4.2. Beryllium

The line list of atomic lines compiled by Primas et al. (1997) was adopted in this work. This same line list was adopted in many analyses of Be abundances in literature (García Pérez & Primas 2006, Primas et al. 1997, 2000a,b, Randich et al. 2002, 2007).

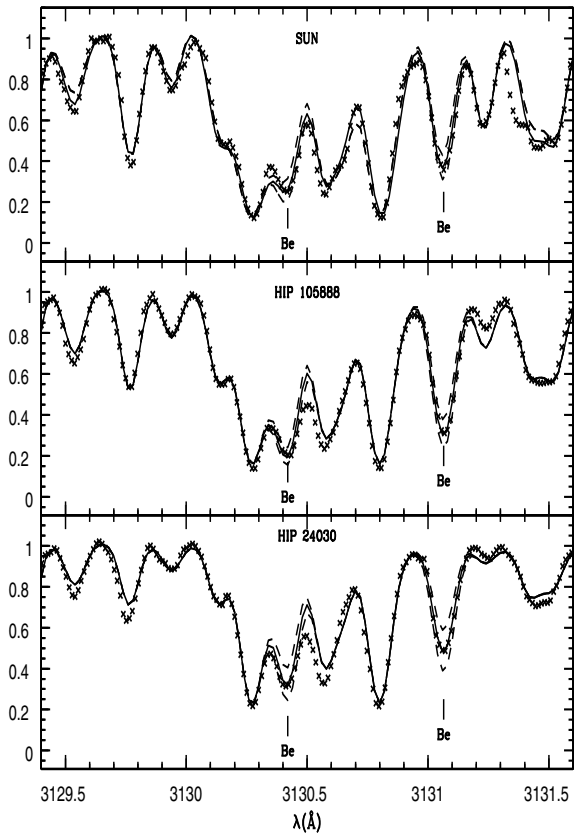

Fig. 2. Fit to the region of the beryllium lines in the solar spectrum and in the stars HIP 105888 and HIP 24030. The crosses represent the observed spectrum, the solid line the best synthetic fit, and the dashed lines represent changes of ±0.20 dex in the Be abundance of the best fit. A solar abundance of A(Be) = 1.10 was determined.

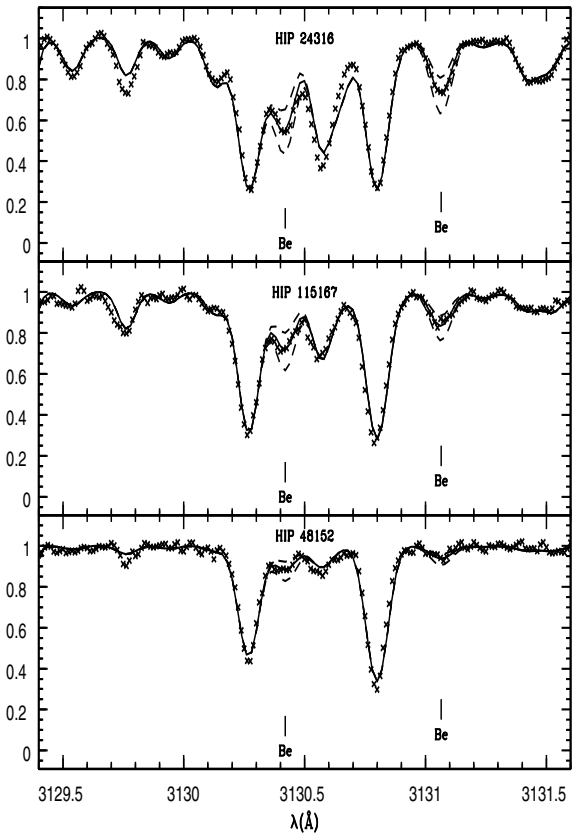

Fig. 3. Fit to the region of the beryllium lines in the stars HIP 24316, HIP 115167, and HIP 48152. The lines are as in Fig. 2.

The adopted log gf of the Be lines are those commonly used in the literature, −0.168 and −0.468 for 3131.065 Å and 3130.420 Å, respectively. In this line list, the blending line affecting the blue wing of the Be 3131 line is assumed to be an Fe I line in 3131.043 Å, with log gf = −2.517 and χ = 2.85 eV. The parameters of this line were constrained using several stars of different parameters and metallicities (see Primas et al. 1997, for details). The proper identification of this line, however, remains controversial in the literature. Castilho et al. (1999), for example, adopt an Fe I line at 3130.995 Å in the analysis of Be in red giants, with log gf = −3.30 and χ = 3.00 eV. Other possibilities explored in the literature include an Mn I line at 3131.037 Å adopted by Garcia Lopez et al. (1995a) and an Mn II line at 3131.015 adopted by Boesgaard & King (2002). In this work, we opted for the Fe I included by Primas et al. (1997), in particular to maintain the consistency with all the papers that adopted the same atomic line list.

There is currently a controversy about a possible missing continuum opacity source affecting the near-UV region, hence Be abundances (Asplund 2004, and references therein). The code used to calculate the synthetic spectra does not include bound-free opacities due to metals (Smiljanic & Barbuy 2007). However, we are mostly interested in relative abundances between stars of similar composition, so the bulk of the analysis is not affected by this uncertainty. The slope between Be and Fe or α could be affected. With respect to this, we note that our most metal-rich stars have [Fe/H] = −0.50; for metal-poor objects, the missing opacity effect is expected to be negligible.

In fact, Balachandran & Bell (1998) argue that the Fe I bound-free opacity should be increased by a factor 1.6. This is equivalent to an increase of 0.20 dex in Fe abundance. We ran a test using the Kurucz suite of codes to test the influence of this increase in Fe abundance in the calculation of Be abundance for a model with [Fe/H] = −0.50, appropriate for star HIP 31639. The difference of 0.022 dex is negligible. We therefore expect that this issue does not really affect our analysis and conclusions in any significant way.

With the line list described above, we fitted the Be lines region in the solar UVES[3] spectrum, adopting the parameters $T_{\rm eff}$ = 5777 K, log g = 4.44, and ξ = 1.00 km s^{-1}, and obtained A(Be) = 1.10 (Fig. 2). This abundance is in excellent agreement with the one found by Chmielewski et al. (1975), A(Be) = 1.15, usually adopted as the reference photospheric solar abundance. We also note excellent agreement with the abundance derived by Randich et al. (2002), A(Be) = 1.11, using this same atomic line list but a different molecular line list and by fitting the Kurucz Solar Flux Atlas (Kurucz et al. 1984).

From the 90 stars in the sample, abundances of Be were determined for 83: 76 detections and 7 upper limits. The 7 stars for which abundances could not be calculated were affected by different problems, some with profiles affected by cosmic rays, and others were found to be spectroscopic binaries. These stars will not be considered further in the analysis. Examples of the fits used to derive the Be abundance are given in Figs. 2 and 3.

For most of the stars, both beryllium lines are well-fitted with the same abundance. In some stars, however, the lines are best

[3] The spectrum is available for download at the ESO website: www.eso.org/observing/dfo/quality/UVES/pipeline/solar_spectrum.html

fitted with slightly different values. In most cases, the difference amounts to ∼0.04 dex, a value that can be completely attributed to the uncertainty of the fitting procedure itself and/or to the determination of the continuum. In one extreme case, however, the difference amounts to 0.24 dex (HIP 31639). This discrepancy is likely due to an inefficient treatment of the blending features caused, for example, by abundance ratios that are significantly different from solar of the blending lines directly affecting the Be lines. For these discrepant cases, we consider the abundance derived solely from the 3131 Å line to be more reliable, since its profile is visually less affected by blends. In Table 3 we list both the beryllium abundance determined solely from the 3131 Å line and the average of the two lines.

We tested the dependence on atmospheric models by also using a version of the Kurucz model atmospheres with enhanced abundances of α-elements, [α/Fe] = +0.40 dex. Metal-poor stars are known to have enhanced abundances of α elements. Some of these elements are particularly important as electron donors and, as such, may influence some continuum opacity sources (bound-free and free-free absorption of H^-, for example). We found, however, this effect to be small. In the following discussion, we adopt the beryllium abundance derived solely from the 3131 line with normal model atmosphere as the reference value.

4.3. Lithium

In our analysis, we expect to recover the initial beryllium abundance the star had at the time of its formation, since this is the one produced by the interaction between the Galactic cosmic-rays (GCR) and the ISM. It is important then to identify stars where significant mixing of the photospheric material with deep hotter regions may have altered the initial Be abundance. The abundances of Li will help in this.

Most stars in our sample have been analyzed for Li abundances before. Our interest in Li in this work is only related to the information it might give on the possible effects of convective mixing, not on the absolute value of the Li abundance. Thus, we decided to adopt Li values from the literature whenever it was available. As main reference for lithium abundances (32 stars), we adopted the work by Charbonnel & Primas (2005), who analyzed a large number of previous literature results in detail. Whenever possible, we adopted their so-called *most consistent values* including NLTE corrections. As a second preferred reference (24 stars), we adopted the results of the survey of Li abundances by Chen et al. (2001). These Li abundances also include corrections for NLTE effects. For stars not included in these papers, the Li abundance was obtained from a number of other papers: for seven stars, abundances were taken from Boesgaard et al. (2005); for four stars, abundances were taken from F00; for three stars, from Romano et al. (1999); while Favata et al. (1996), Gratton et al. (2000), Ryan & Deliyannis (1995), Spite et al. (1994), and Takeda & Kawanomoto (2005) each contributed with one star.

Lithium abundances were not available in the literature for 15 stars of our sample. For these stars, we present new abundances derived using spectral synthesis. We adopted the atomic data for the Li I doublet and neighboring lines listed by Andersen et al. (1984). The Li abundance of star HIP 92781 could not be calculated because of a damaged profile. The lithium abundances are listed in Table 3 along with a flag indicating the sources. An example of a synthetic fit to the Li I doublet is shown in Fig. 4.

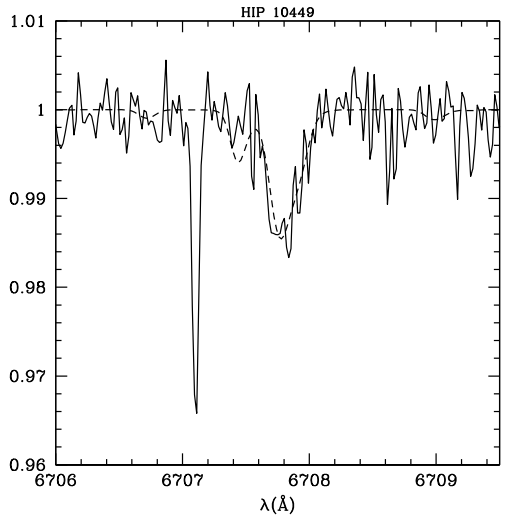

Fig. 4. Fit to the Li I doublet at 6707.8 Å in star HIP 10449. The solid line is the observed spectrum and the dashed line the synthetic one.

Since Li and Be are destroyed at different depths, even stars depleted in Li are expected to have preserved their original Be abundance (as is likely in the case of the Sun and of cool main sequence stars, cfr. e.g. Randich 2007). Whatever the Li reference adopted, non-mixed metal-poor dwarfs are expected to have a lithium abundance close to the primordial value of the Spite plateau (Spite & Spite 1982). The exact value of the plateau and possible dependencies with [Fe/H] and/or $T_{\rm eff}$ are still controversial, but for our purpose it is sufficient to assume a typical value of A(Li) = 2.20.

4.4. Alpha elements

Abundances for the α-elements were taken from the work of Venn et al. (2004). These are average abundances of Mg, Ca, and Ti determined in the same papers, when available, used as the source of the atmospheric parameters we adopt in this work. The abundances have not been homogenized since different works use different spectral lines to calculate the abundances. We refer the reader to Venn et al. (2004) and the original papers for more details. We list the abundances in Table 6. We plan to improve this analysis by evaluating CNO abundances for all the stars in a subsequent work (Smiljanic et al. 2009, in preparation).

4.5. Uncertainties

Beryllium

The Be abundance determination is affected by the uncertainty in the atmospheric parameters and uncertainty in the determination of the pseudo-continuum. To estimate the effect of the atmospheric parameters, we change each one by its own error, keeping the other ones with the original adopted values, and recalculate the abundances. Thus, we measure what effect the variation of one parameter has in the abundances. These effects are listed in Table 7. The calculations were done for three stars representative of the range of parameters defined by our sample. The total uncertainty also includes the effect of the continuum uncertainties (±0.05 dex) and the influence of the unidentified blends (±0.08 dex) on the Be abundance. We recall that we adopted larger uncertainties for $T_{\rm eff}$ and [Fe/H] when compared to the values adopted by F00 and Ed93. Thus, the uncertainties caused

Table 7. The uncertainties of the Be abundance introduced by the uncertainties of the atmospheric parameters.

Star	$\sigma_{T_{eff}}$	$\sigma_{\log g}$	σ_{ξ}	$\sigma_{[Fe/H]}$	$\sigma_{cont.}$	σ_{blend}	σ_{total}
HIP 53070	±0.03	±0.06	±0.01	±0.00	±0.05	±0.08	±0.12
HIP 104660	±0.03	±0.08	±0.01	±0.02	±0.05	±0.08	±0.13
HD 159307	±0.04	±0.08	±0.01	±0.03	±0.05	±0.08	±0.13

Table 8. The uncertainties of the Li abundances, calculated in this work, introduced by the uncertainties of the atmospheric parameters.

Star	$\sigma_{T_{eff}}$	$\sigma_{\log g}$	σ_{ξ}	$\sigma_{[Fe/H]}$	$\sigma_{cont.}$	σ_{total}
HIP 74067	±0.10	±0.00	±0.00	±0.00	±0.05	±0.11

The total uncertainty also includes the effect of the continuum uncertainties (±0.05 dex) on the Li abundance.

by these parameters in the abundances already consider some of the effects of putting the two samples together.

The uncertainty due to the continuum was determined by estimating the sensitivity of the derived Be abundance on the continuum level adopted. This uncertainty is mostly related to the S/N of the spectrum. After a number of tests with different choices for the continuum level, we found this effect to introduce a typical uncertainty of ±0.05 dex.

Another factor that may influence the determination of Be abundances are the blends affecting the Be lines. In particular, we adopt the value given only by the 3131 Å line as the abundance. In this case, the predicted line of Fe I is the most important blend. The influence of this predicted line decreases with increasing temperature and/or decreasing metallicity. In a series of tests, we noticed that removing the Fe line would increase the beryllium abundance in a star with $T_{eff} \sim 5200$ K and metallicity ~ -0.90 by 0.15 dex. In a star with $T_{eff} \sim 6200$ K and metallicity ~ -0.70, no effect is seen at all. We adopt a value of ±0.08 dex, the average between the maximum and minimum effect of neglecting blend, to represent this source of uncertainty and extend this value to all the sample stars. If our tentative identification of the line is wrong, we are wrongly modeling the effects of its variation with [Fe/H] and Teff. This effect, however, is not likely to be as strong as the complete neglect of the line.

Assuming that the effects of the uncertainties from the parameters, the continuum, and the blends are independent, we may add them in quadrature to estimate the total uncertainty, which is also listed in Table 7.

Lithium

In the case of lithium, the main uncertainties also come from the uncertainties in the atmospheric parameters and from the determination of the pseudo-continuum. These uncertainties were determined in a similar way to the one described above for Be and are listed in Table 8. While the main parameter affecting the abundance is log g for Be, for Li it is T_{eff}. The uncertainties we derive are only valid for the Li abundances determined in this work, for the values adopted from the literature we refer the reader to the original papers.

Alpha elements

As in Venn et al. (2004), we do not conduct a detailed error analysis on the α-elements since they were determined from a variety of indicators. We decided to adopt the same representative uncertainty as adopted by Venn et al. (2004), $\sigma_{[\alpha/Fe]} = \pm 0.15$ dex.

5. Comparison with previous results

A number of the stars analyzed in this work have beryllium abundances previously determined in the literature. A detailed comparison of our results with those obtained previously for each star is shown in Appendix A for the interested reader. As is clear from this comparison, there is also a difference in log g in most cases where our abundances do not agree with previous results. This shows that to establish a consistent and reliable gravity scale is important for properly determining the Be abundance. We have confidence in our results given the good agreement found with log g derived using the Hipparcos parallaxes.

In the following, we discuss both the spread in the atmospheric parameters between the results found in these papers (in particular the one of [Fe/H], that might have some influence in the spread of the relation between Be and Fe) and the spread of the Be abundances. The spread of Be abundances might show to what extent the absolute scale of the abundances is reliable.

5.1. The spread of the parameters

Although in the comparison shown in Appendix A we show results from all papers that previously determined Be abundances for our sample stars, in what follows we consider only papers published after 1997 (including). Early works most likely employed data and techniques of lower quality then modern analyses and therefore are prone to greater uncertainties. We also do not consider upper limits for this comparison, resulting in 25 possible comparisons. Multiple comparisons for a given star are possible.

The average difference between our log g values and the ones adopted in the literature is 0.00 ± 0.28. If we exclude the comparison of our log g of HIP 114962, 4.30, with the one adopted by Molaro et al. (1997a), 3.44, the average is −0.03 ± 0.23. This shows that, although no systematic effect seems to be present, a wide spread of the log g values adopted in the literature exists.

Regarding the metallicity, [Fe/H], the average difference between our values and the ones adopted in the literature is +0.12 ± 0.19. If again we exclude the comparison with of HIP 114962 by Molaro et al. (1997a), the average is +0.13 ± 0.17. This comparison seems to indicate a weak systematic effect in the sense of our adopted [Fe/H] values to be higher then the ones adopted in other analyses. It also indicates the existence of a spread of the [Fe/H] values adopted in the literature. This spread is a measure of the extent to which the determinations can be considered reliable. It will be important to keep this in mind when we discuss the relation between log(Be/H) and [Fe/H] in the sections to follow. We note that the the uncertainty we

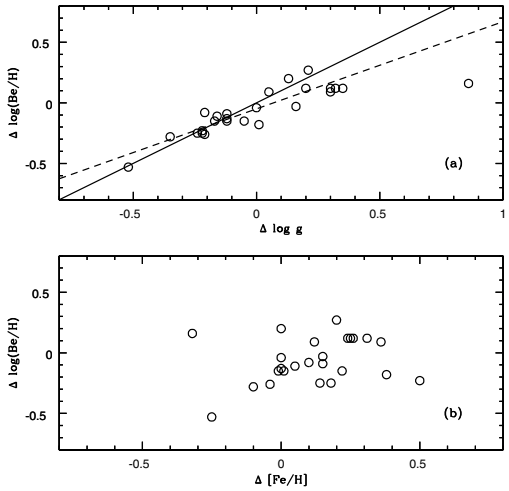

Fig. 5. a) Diagram showing the difference between the Be abundances determined in this work and the ones from the literature, as a function of the difference in log g. The correlation coefficient, $\rho = 0.84$, including the outlier, and $\rho = 0.90$, excluding it, indicates the reality of the linear correlation apparent from the figure. The dashed line indicates a linear fit, excluding the outlier, and the solid line is the line $x = y$. **b)** The difference between the Be abundances as a function of the difference in [Fe/H]. The correlation coefficient, $\rho = 0.24$, indicates the lack of correlation as apparent from the figure.

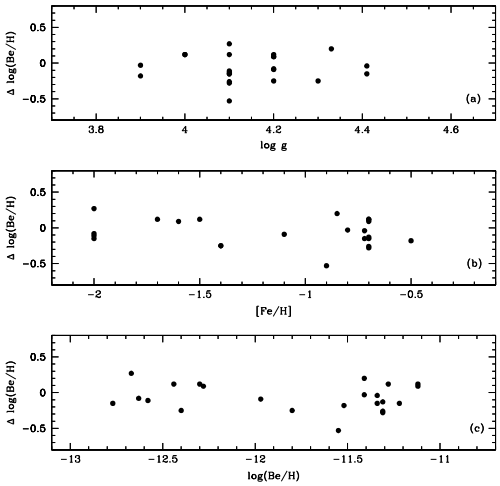

Fig. 6. a) Diagram showing the difference between the Be abundances determined in this work and the ones from the literature, as a function of the log g values. The correlation coefficient, $\rho = 0.14$, indicates the lack of correlation also apparent from the figure. **b)** The difference between the Be abundances as a function of the [Fe/H] values. The correlation coefficient, $\rho = -0.26$, indicates the lack of correlation also apparent from the figure. **c)** The difference between the Be abundances as a function of the log(Be/H) values. The correlation coefficient, $\rho = -0.20$, indicates the lack of correlation also apparent from the figure.

assume for the [Fe/H] values is similar to the magnitude of the spread found in this comparison.

5.2. The spread on the Be abundances

The average difference between our Be abundances and the ones determined in the literature is -0.06 ± 0.19. This indicates that, on average, our values are slightly lower than the ones previously derived in the literature. As shown in Fig. 5, the difference in the Be abundance correlates very well with the difference in log g but not with the difference in [Fe/H]. This comparison shows the extent to which different analyses of Be can be trusted when compared to each other. It also shows that most of this spread is related to the difference in the adopted log g. Also, no correlation between the difference in the Be abundance and the own abundance, [Fe/H], and log g was found (Fig. 6). Therefore, this difference does not seem to be due to some systematic effect of the analysis. As shown before, our log g values are in excellent agreement to the ones derived using Hipparcos parallaxes, giving confidence in the abundances we derived.

6. Be depleted stars

The light elements Li, Be, and B are very fragile and are destroyed when in regions inside stars with temperatures of 2.5×10^6 K, 3.5×10^6 K, and 5×10^6 K, respectively. Main-sequence stars with $M \lesssim 1.5\ M_\odot$ have a surface convective zone that might reach regions hot enough to deplete the surface abundance of these elements. The depth of the convective zone is a function of effective temperature and metallicity; it is larger when the star is cooler and more metal-rich.

In this section we use Li and Be abundances to evaluate which stars are affected by some kind of mixing event. The stars that do not display the original Be abundances in their photospheres will be excluded from further discussion. We also exclude star HIP 59490, the Be-rich star discussed in detail in Smiljanic et al. (2008). Both Li and Be abundances of this star are not a result of the normal evolution of these elements in the Galaxy, but a likely result of a peculiar event tentatively identified as a hypernova.

Seven stars in our sample have only Be upper limits. All have also low Li abundances. Three of them are subgiants, HIP 17001, HIP 71458, and HIP 77946, and have probably diluted both Li and Be due to the deepening of the convective envelope, as expected from stellar evolution. One is HIP 55022 (HD 97916), a star first found to be Li depleted by Spite et al. (1984). It is one of the so-called "ultra-lithium-deficient" stars (Ryan et al. 2001), a group of a few metal-poor stars that deviate from the Li plateau and only have Li upper limits. Ryan et al. (2001) suggest they are formed by the same mechanism as forms field blue stragglers. Boesgaard (2007) find these stars are also Be-depleted, a result we confirm for HIP 55022. The thick-disk dwarf HIP 59750 is more metal rich ([Fe/H] = −0.60) than the stars that usually define the Li plateau. At its temperature (6200 K), no Li (or Be) depletion is expected. Star HIP 36818 has a lower temperature (5672 K) and higher metallicity ([Fe/H] = −0.83) than plateau stars. Stars of similar temperature and metallicity also show Li depletion but normal Be. Both seem to be affected by stronger mixing than other similar stars. They might as well be metal-rich counterparts of the "ultra-lithium-deficient" stars mentioned above. Star HIP 19814 has a rather high Be upper limit, consistent with stars of similar temperature and metallicity where Be was detected. Thus, strictly speaking it cannot be considered to be Be-depleted. All these 7 stars will not be considered in the discussion presented in the following sections. We thus start with a sample of 75 stars where Be was detected.

Spite & Spite (1982) were the first to show halo stars with a range of metallicity to have a constant Li abundance (the so-called Spite plateau). Thick-disk, metal-poor dwarfs also show the same feature (Molaro et al. 1997b). Although departures

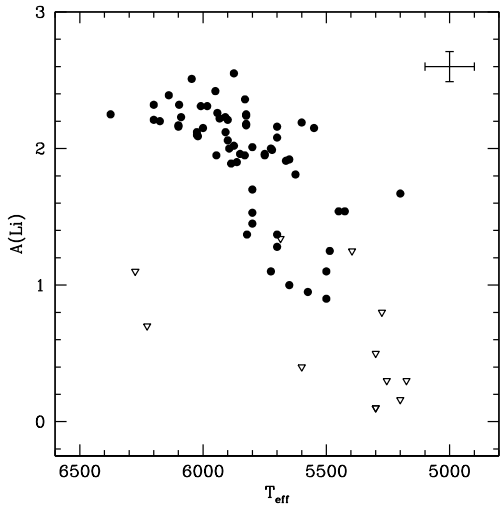

Fig. 7. Abundances of Li as a function of temperature for the sample stars. Detections are shown as filled circles and upper limits as upside down open triangles.

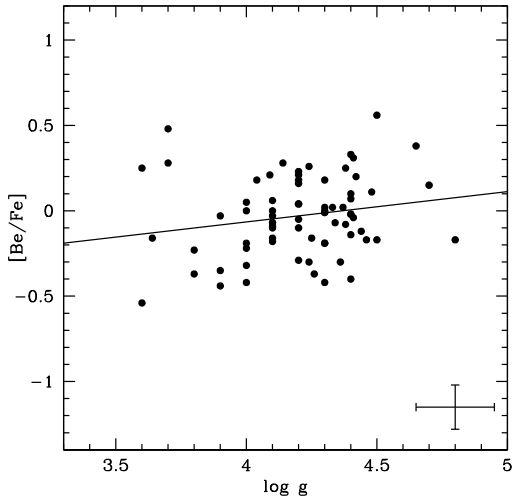

Fig. 8. Abundances of Be relative to Fe as a function of log g for the sample stars. A linear fit to the points is also shown.

from the plateau due to lithium production by various stellar sources seem to start at [Fe/H] ~ -1.00, a sudden large increase with stars reaching A(Li) $\sim$ 3.0 is observed only for [Fe/H] > -0.45, out of the explored range (Travaglio et al. 2001). Although some discussion exists on whether the plateau is primordial in origin or a result of some depletion mechanism (Bonifacio & Molaro 1997; Piau et al. 2006; Bonifacio et al. 2007; Korn et al. 2007), we assume in this work that plateau stars did not suffer a previous significant depletion of Li (and Be) in their atmospheres.

In Fig. 7 we show the lithium abundances as a function of $T_{\rm eff}$. As previously found in the literature, stars with $T_{\rm eff} \gtrsim 5800$ K define the Li plateau, while stars with $T_{\rm eff} \lesssim 5800$ K start to show the effects of Li depletion. There are only two stars with $T_{\rm eff}$ above 6000 K and A(Li) below the plateau. HIP 85963 is a thin-disk star with [Fe/H] $= -0.71$, $T_{\rm eff} = 6227$, and A(Li) $\leq$0.70, and HIP 107975 is a thin-disk star with [Fe/H] $= -0.50$, $T_{\rm eff} = 6275$, and A(Li) $\leq$1.10. Both seem to be lithium-dip[4] stars or to be evolving from the lithium dip. Since they have most likely experienced strong mixing, we do not consider them in the further analysis, reducing our sample to 73 stars. Similar plots of A(Li) as a function of log g and [Fe/H] do not reveal any other star showing strong mixing.

No trends or deviating stars are seen in plots of [Be/Fe][5] as a function of $T_{\rm eff}$ and [Fe/H]. We use [Be/Fe] in this case because log(Be/H) is expected to vary from star to star, while [Be/Fe] is expected to be roughly constant. A small trend with a correlation coefficient of $\rho = 0.19$ is seen in a plot of [Be/Fe] as a function of log g (Fig. 8), suggesting a small decrease in Be abundance with decreasing log g. Stars with log $g \geq 4.00$ seem to form a plateau, while some stars with log $g < 4.00$ seem to have low [Be/Fe]. A similar effect is not seen in the Li abundances,

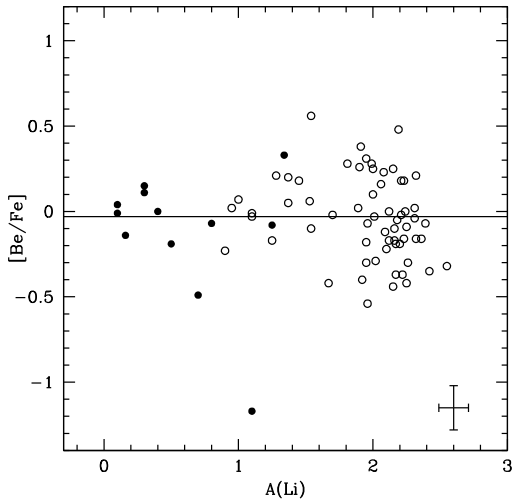

Fig. 9. The [Be/Fe] ratio as a function of the Li abundance. Stars with beryllium abundances but lithium upper limits are shown as filled circles and stars with both beryllium and lithium detections are shown as open circles. A linear fit to the points, without the excluded stars, is also shown. No correlation between the abundances of Li and Be is seen.

which argues against a simple dilution or mixing effect. These stars span almost the whole range of metallicity (from -0.50 to -1.80), which argues against a chemical evolution effect. The trend might be related to the dependence of Be on gravity, suggesting that log g for the lower gravity stars is possibly not well constrained. Nevertheless, we see no strong reason to exclude these stars from the discussion.

Thus, only two stars are excluded from the sample because of possible mixing effects. The remaining 73 stars retain their original Be abundances and are used in the following sections to discuss the galactic evolution of this element and the use of Be as a time scale tracing the different star formation history of the halo and the thick disk.

Finally, in Fig. 9 we plot the [Be/Fe] as a function of the lithium abundances. No clear trend between Be and Li is seen. The stars with lower Be abundance are not the ones with smaller Li abundance. Actually, most of the stars with Li upper-limits

[4] The so-called lithium-dip is a strong decrease in Li abundances of main sequence stars in an interval of ~300 K around ~6700 K, an effect first noticed by Wallerstein et al. (1965) in the Hyades and later confirmed by Boesgaard & Tripicco (1986). A discussion of the physical mechanisms possibly associated to the lithium dip can be found in Charbonnel & Talon (1999, and references therein).

[5] We adopt the meteoritic solar abundance, A(Be)$_\odot$ = 1.41 (Lodders 2003) to calculate the [Be/Fe] ratio.

have Be abundances compatible with stars that show no signs of Li depletion. We note that three stars for which we determined only a Be upper limit have Li detection, however, they are cool, $T_{\rm eff} < 5500$ K and Li-depleted relative to the plateau. This is probably a result of the much higher S/N obtained in the red regions of the spectra. These stars are nevertheless very interesting and should be further investigated.

7. Galactic evolution of Be

Once we have cleaned our original sample by identifying the stars that have suffered Be dilution or depletion, or for which we cannot determine Be abundances, we can investigate the evolution of Be in the Galaxy. We are left with 73 stars, 6 from the thin disk, 27 from the thick disk, and 39 from the halo. One star has a 50% probability of being either halo or thick disk. We keep this star and the thin disk stars in the sample because according to different kinematic criteria they receive a different classification (such as in the dissipative and accretion components defined by Gratton et al. 2003a – see below). In Fig. 10 we show a diagram of the [Fe/H] vs. log(Be/H) and in Fig. 11 a diagram of [α/H] vs. log(Be/H) for all the 73 stars. In both figures, the points are distributed along linear relations, as previously found in the literature. We fitted a straight line to the data, taking the errors on both axes into account. Following the discussion in Sect. 5 we adopted an error of 0.15 dex on [Fe/H] and [α/H]. The adopted error on the Be abundance was 0.13 dex. The resulting fits are the following:

$$\log(\mathrm{Be/H}) = (-10.38 \pm 0.08) + (1.24 \pm 0.07)\,[\mathrm{Fe/H}] \quad (1)$$

$$\log(\mathrm{Be/H}) = (-10.62 \pm 0.07) + (1.36 \pm 0.08)\,[\alpha/\mathrm{H}]. \quad (2)$$

For the fit with [Fe/H] the goodness-of-fit provides a probability of 0.14, while for the one with [α/H] this is 0.76. Although both fits are formally acceptable, the difference in goodness-of-fit between the two is remarkable. The probability is very sensitive to the error estimates. If we decrease our error estimate on [Fe/H] and [α/H] to 0.12 dex, the probability of the two fits drops to 0.002 and 0.14 respectively. Therefore, while the linear fit with [α/H] remains acceptable, the one with [Fe/H] would not, generally, be considered acceptable. Visual inspection of Figs. 10 and 11 confirms the impression derived from the statistical analysis. While in Fig. 11 one can see a clear trend, albeit with an obvious scatter, one has the impression in Fig. 10 of being able to see two parallel linear relations.

The most important relation to study the chemical evolution of Be is the one with [O/H], since oxygen gives the highest contribution to the spallation process responsible for forming Be. In the absence of oxygen abundances for our complete sample, we decided to use the average abundance of α-elements, as compiled by Venn et al. (2004). These are typically an average of Mg and Ca; when available Ti also enters into the definition of α by Venn et al. (2004). These elements show behavior with metallicity similar to oxygen. It is therefore reasonable to use [α/H] as a proxy for [O/H]. No major inconsistency should be introduced by this choice. That a single linear relation links Be and α elements, even when considering stars extracted from different Galactic populations (halo, thick disk, thin disk) is a consequence of the uniqueness of the physical process leading to Be formation. A non-uniqueness of the relation between Be and Fe, if present, could be a consequence of the different evolution of Fe in the different Galactic populations.

In Table 9 we compare the linear relations we derived with the ones previously obtained in the literature for metal-poor stars. The relation with oxygen or α-elements shows a sizable scatter in the fitted slope; this is likely due to the difficulty in the measurement of oxygen abundances in metal-poor stars. Our own slope is close to the ones obtained by King (2002) using [Ca/H] and Boesgaard et al. (1999) using [O/H]. The zero points seem to agree better, the exception being the one determined by King (2002) using [Ca/H]. Our own value is the same as obtained by King (2001) and Molaro et al. (1997a) both using [O/H]. The slope with the α-elements abundance implies the need for a primary production of Be. All the relations with Fe have a slope very close to one. The zero points of the fits have a larger scatter. The zero point of our fit is closer to the one obtained by King (2001), who analyzed results available in the literature.

The possible presence of a real scatter in the Be-Fe relationship needs to be considered further. The spread is also present in earlier data samples but, the limited size of the samples and the large errors on Be abundance did not allow a robust assessment of its existence. In particular, the presence of this scatter

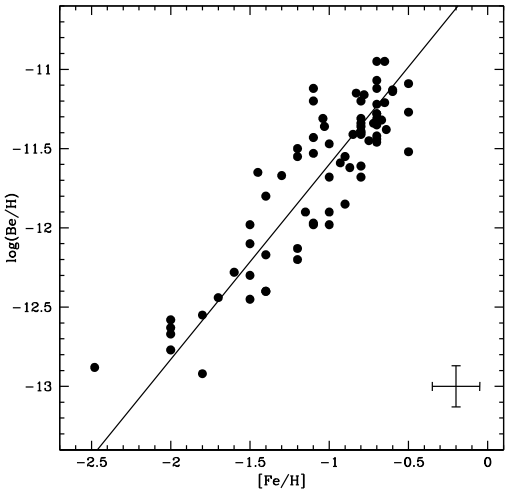

Fig. 10. Diagram of [Fe/H] vs. log(Be/H) for all the 73 stars showing a linear fit to the points. A correlation coefficient of $\rho = 0.89$ is found. An example of error bar is shown in the *lower right corner*.

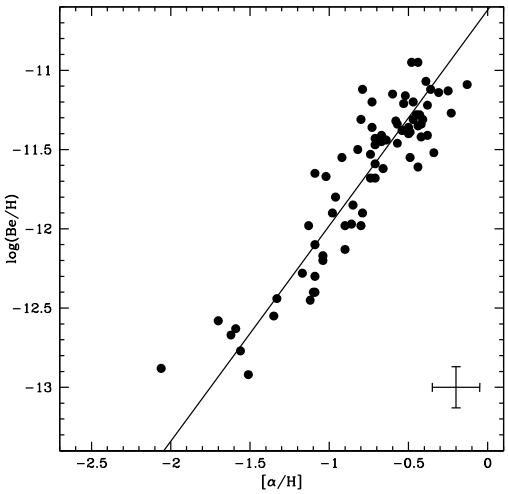

Fig. 11. Diagram of [α/H] vs. log(Be/H) for all the 73 stars showing a linear fit to the points. A correlation coefficient of $\rho = 0.91$ is found. An example of error bar is shown in the *lower right corner*.

Table 9. A comparison of the linear relations between Be and Fe and O (or any other α indicators adopted) as found in the literature.

log(Be/H) = (A $\pm\sigma_A$) + (B $\pm$ σ_B) [Fe/H]	Ref.
log(Be/H) = (−10.38 ± 0.08) + (1.24 ± 0.07) [Fe/H]	This work (all stars)
log(Be/H) = (−10.34 ± 0.09) + (1.27 ± 0.08) [Fe/H]	This work (F00 stars)
log(Be/H) = (−10.40 ± 0.08) + (1.22 ± 0.07) [Fe/H]	This work (halo stars)
log(Be/H) = (−10.38 ± 0.08) + (1.16 ± 0.07) [Fe/H]	This work (thick disk stars)
log(Be/H) = (−10.22 ± 0.07) + (1.16 ± 0.04) [Fe/H]	King (2001)
log(Be/H) = (−10.59 ± 0.03) + (0.96 ± 0.04) [Fe/H]	Boesgaard et al. (1999)
log(Be/H) = (−10.19 ± 0.11) + (1.07 ± 0.08) [Fe/H]	Molaro et al. (1997a)
log(Be/H) = (−9.76 ± 0.22) + (1.26 ± 0.11) [Fe/H]	Boesgaard & King (1993)
log(Be/H) = (−10.87 ± 0.51) + (0.77 ± 0.23) [Fe/H]	Gilmore et al. (1992)[2]
log(Be/H) = (A ± σ_A) + (B ± σ_B) [α/H]	Ref.
log(Be/H) = (−10.62 ± 0.07) + (1.36 ± 0.08) [α/H]	This work (all stars)
log(Be/H) = (−10.71 ± 0.07) + (1.34 ± 0.08) [α/H]	This work (F00 stars)
log(Be/H) = (−10.62 ± 0.07) + (1.37 ± 0.08) [α/H]	This work (halo stars)
log(Be/H) = (−10.64 ± 0.07) + (1.31 ± 0.08) [α/H]	This work (thick disk stars)
log(Be/H) = (−10.87 ± 0.28) + (1.10 ± 0.18) [Mg/H]	King (2002)
log(Be/H) = (−10.33 ± 0.16) + (1.31 ± 0.18) [Ca/H]	King (2002)
log(Be/H) = (−10.61 ± 0.06) + (1.51 ± 0.05) $[O/H]^1_{mean}$	King (2001)
log(Be/H) = (−10.69 ± 0.04) + (1.45 ± 0.04) [O/H]	Boesgaard et al. (1999)
log(Be/H) = (−10.62 ± 0.13) + (1.13 ± 0.11) [O/H]	Molaro et al. (1997a)
log(Be/H) = −10.68 + 1.12 [O/H]	Boesgaard & King (1993)
log(Be/H) = (−11.19 ± 0.25) + (0.85 ± 0.15) [O/H]	Gilmore et al. (1992)[2]

[1] A mean oxygen abundance from different indicators, such as the molecular OH UV lines and the λ6300 [OI] forbidden line; [2] the fits were recalculated in this work based on the original published data.

in samples of smaller size might have motivated the claim of a change in the slope, as in Molaro et al. (1997a) and Boesgaard et al. (1999). Molaro et al. (1997a) were the first to suggest a possible change in the slope of the relation of Be with Fe at [Fe/H] ∼ − 1.6, −1.1. No such change is apparent in our data.

In the hypothesis that Be is a good cosmochronometer, there could be a natural explanation for the scatter. At a given time in the early-Galaxy, the Galactic halo has a higher metallicity than the thick disk. Thus, a star formed at this time in the halo will have a higher [Fe/H] than a star formed at the same time in the thick disk, in spite of a similar Be abundance. We devote the next sections to a detailed investigation of the presence of the scatter and to its possible causes. This investigation will help to constrain the limits of validity of Be as a cosmochronometer.

7.1. Scatter in the Be-Fe relation

In Fig. 12 we display our working sample of 73 stars, using different symbols to identify several subsets. In addition in the plot the two stars, HD 94028 and HD 132475, identified by Boesgaard & Novicki (2006) to lie at about 4σ above the mean Be-Fe trend are also shown. In this sense these two stars must be considered Be-rich. However, we note that HD 94028 is also included in our sample. While Boesgaard & Novicki (2006) find log(Be/H) = −11.49, we derived log(Be/H) = −11.80 and thus do not confirm the "Be rich status" of this star. Although the results basically agree within 1σ (we estimate ±0.13 dex for our results and Boesgaard & Novicki ±0.12 for theirs), the difference is associated to the different log g values adopted, log g = 4.20 by us and log g = 4.44 by Boesgaard & Novicki. The log g derived using the Hipparcos parallax is log g = 4.27. As we point out in Sect. 5, correct determination of log g is essential for deriving consistent Be abundances. In Fig. 13 we show our fit to the spectrum of this star and a synthetic spectrum calculated with the larger abundance found by Boesgaard & Novicki (but calculated with our adopted atmospheric parameters). Another, even more striking example of Be-rich star is HD 106038 (=HIP 59490, Smiljanic et al. 2008), which we have removed from our analyzed sample. Boesgaard & Novicki (2006) suggests that large Be abundance arises from local enrichment phenomena, such as may happen in "Super Bubbles" in the vicinity of a Supernova

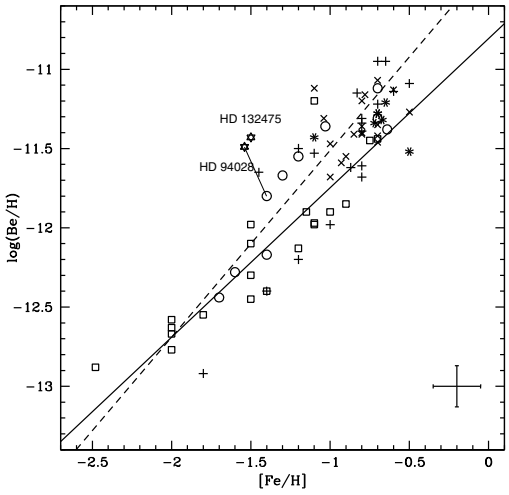

Fig. 12. Our sample of 73 stars in the [Fe/H] – log(Be/H) plane split in several sub samples. Circles are thick-disk stars with A(Li) ≥ 2.0, squares halo stars with A(Li) ≥ 2.0, × symbols are thick-disk stars with A(Li) < 2.0 and + symbols are halo stars with A(Li) < 2.0. Asterisks are thin-disk stars or stars with ambiguous kinematic classification. The two star symbols are the Be-rich stars HD 94028 and HD 132475 from Boesgaard & Novicki (2006). HD 94028 (HIP 53070) is also included in our sample, where a smaller Be abundance was derived. A short line connects the two values. The solid line is a least squares fit to the open square symbols and the dashed line is a least squares fit to the open circles symbols. A representative error bar is shown at the bottom right of the plot.

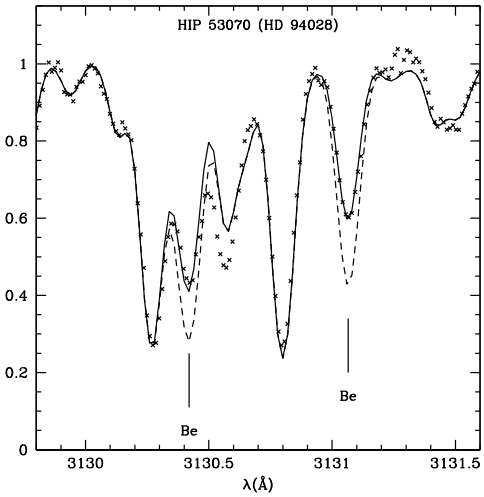

Fig. 13. Fit to the region of the beryllium lines in star HIP 53070 (HD 94028). The crosses represent the observed spectrum, the solid line the best fit, and the dashed line a synthetic spectrum calculated with our adopted atmospheric parameters and the beryllium abundance determined by Boesgaard & Novicki (2006), log(Be/H) = −11.49.

(see Parizot 2000; Parizot & Drury 2000 and references therein). For the large Be enhancement of HD 106038, Smiljanic et al. (2008) found such a scenario insufficient and invoked a hypernova. Such Be-rich stars seem to be quite rare, and at present it seems unlikely that they contribute to a large scatter in Be abundances. The Galactic orbits of all three stars have been computed by Caffau et al. (2005) and while HD 132475 and HD 106038 are halo stars, HD 94028 displays a disk-like kinematics. This suggests that the events giving rise to Be-rich stars are indeed quite local and do not depend on the stellar population to which the star belongs.

Inspection of Fig. 12 gives the visual impression that squares and circles (halo and thick disk) define two distinct linear relations. At the same time it is clear that the Li-depleted stars would blur this picture, especially those belonging to the halo. This is confirmed by fitting a straight line to the halo stars alone. The fit to all the halo stars (39 stars) has a probability of 0.04, marginally acceptable, but suspicious. If we remove from the sample all the Li-depleted stars we are left with a sample of 20 stars, and the probability of the fit jumps up to 0.19. This fit is shown in Fig. 12 corresponding to

$$\log(\mathrm{Be/H}) = (-10.76 \pm 0.15) \; + \; (0.97 \pm 0.10)\,[\mathrm{Fe/H}]. \qquad (3)$$

The sample of thick-disk stars, on the other hand, shows a reasonable fit (0.69 probability) without the need to remove the Li-depleted stars. The fits obtained by keeping all the thick-disk stars and by removing the Li-depleted stars are very similar. For consistency in Fig. 12 we give the one without Li-depleted stars, which corresponds to

$$\log(\mathrm{Be/H}) = (-10.30 \pm 0.25) + (1.21 \pm 0.20)[\mathrm{Fe/H}]. \qquad (4)$$

The choice of eliminating the halo Li-depleted stars from the fit is somewhat arbitrary and we have no particular justification for it. Even more so, if we note that many of the halo Li-depleted stars have Be abundances that are *higher* than the mean trend defined by the other stars. It is nevertheless remarkable that making this choice the goodness-of-fit increases.

Our conclusion is that there is marginal evidence of scatter in the Be-Fe relation, above what can be justified by observational errors. One possibility is that two distinct Be-Fe relations exist: one for the halo and one for the thick disk. Another possibility is that there is simply a dispersion in Be abundances at any given metallicity.

7.1.1. Stars with similar parameters

We are analyzing a set of high quality data of stars that have, for the vast majority, parallaxes measured by Hipparcos and have been quite extensively studied in the literature. Nevertheless, we are aware that the uncertainties in an abundance analysis are often underestimated.

We believe a meaningful test of the existence of real scatter is to identify stars with similar metallicity and similar atmospheric parameters, hence almost identical spectra, but different Be abundances. The difference in strength of the Be lines should be obvious and largely independent of our ability to model the spectra.

We identified 4 pairs of stars with similar atmospheric parameters and metallicities. Their spectra are compared in Fig. 14. In this figure, all the pairs of spectra show very good agreement in the behavior of the neighboring metal lines, but clearly differ in the two Be lines. This difference is a definitive and convincing test that the scatter in the abundances is a real feature. The stars being compared range from [Fe/H] = −0.80 to −1.40, showing that the scatter is not concentrated in a single metallicity value, the stars in each pair have very similar gravities, as well as similar Li abundances. We cannot therefore invoke differences in gravity or in dilution/depletion to explain the observed Be difference.

The situation for α elements is less clear. In the above pairs of stars, the [α/H] ratio is not the same, so we could expect stars with the same metallicity but different oxygen abundance to have different Be abundances. It is more difficult to identify stars in our sample with similar atmospheric parameters and also the same [α/H], but different Be. Of the stars in Fig. 14, HIP 22632 and HIP 53070 are the ones with the the most similar [α/H], −1.04 and −0.96 dex, respectively. In Fig. 15 we compare two calcium lines, λ6166.44 Å and λ6169.04 Å of these stars. As is clear from this figure, there is no difference in the calcium abundances of these stars. The difference in α-element abundances of the other stars in Fig. 14 are on the order of −0.15, which is close to the 1σ uncertainty of the abundances. The case of HIP 22632 and HIP 53070 shows that stars with similar abundances of α-elements may have different abundances of Be.

7.1.2. Binaries

We have finally investigated some other possible factors that may influence the scatter, such as the use of data from different sources or the possible presence of binaries. We collected information on the multiplicity of our sample stars in the literature, which is listed in Table 1, where whenever possible we list the number of components of the system (AB for two components, ABC for three, and so on). When the number of stars in the system was not clear we only list a flag *yes* to indicate the star is a binary or multiple system. The references consulted employed a variety of methods, for example, radial velocities, photometry, or speckle interferometry. A flag *no* does not necessarily mean the star is single, but that a reference was found where at least one method failed to detect multiplicity. For some stars no reference reporting an investigation on multiplicity was found, in this case no flag is shown in the table. Again, no difference between

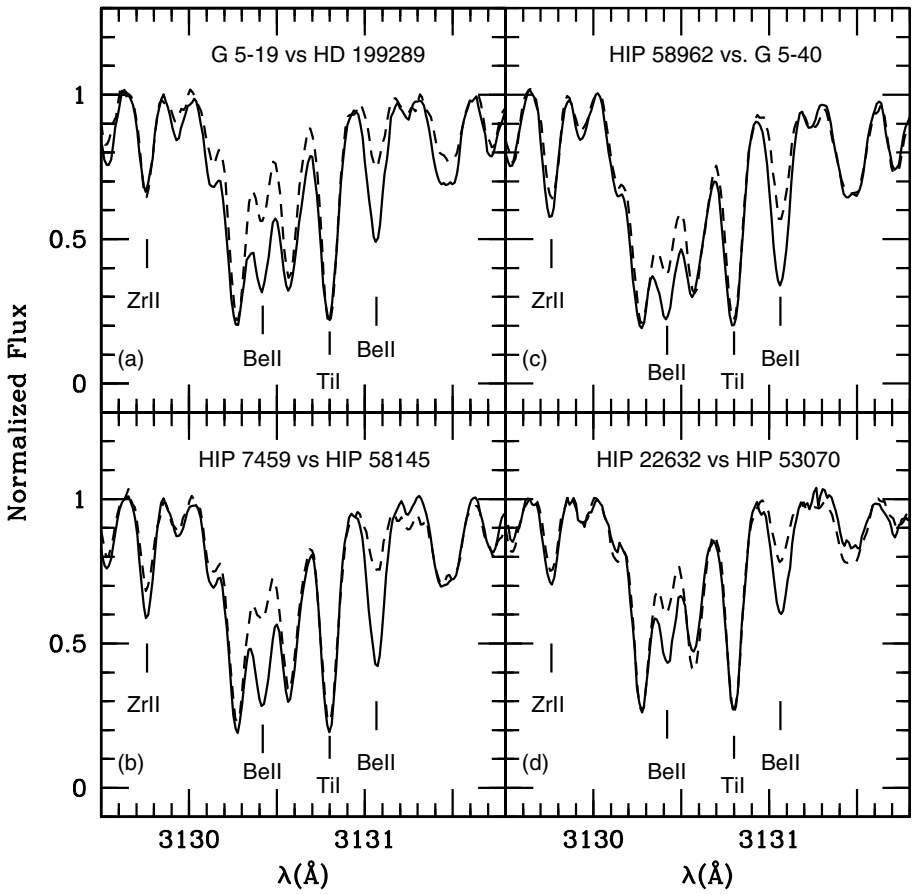

Fig. 14. Comparison in the Be region between spectra of stars with similar metallicity but different Be abundances. **a)** G 5–19 with $T_{\rm eff}$/ log g/[Fe/H]/log(Be/H) = 5942/4.24/- 1.10/-11.98, shown as a dashed line, vs. HD 199289 with $T_{\rm eff}$/log g/[Fe/H]/log(Be/H) = 5894/4.38/-1.03/-11.36, shown as a solid line. **b)** HIP 7459 with $T_{\rm eff}$/ log g/[Fe/H]/log(Be/H) = 5909/4.46/-1.15/-11.90, dashed line, vs. HIP 58145 with $T_{\rm eff}$/ log g/[Fe/H]/log(Be/H) = 5946/4.41/-1.04/-11.31, solid line. **c)** HIP 58962 with $T_{\rm eff}$ / log g/[Fe/H]/log(Be/H) = 5831/4.36/−0.80/−11.68, dashed line, vs. G 5-40 with $T_{\rm eff}$/log g/[Fe/H]/log(Be/H) = 5863/4.24/−0.83/−11.15, solid line. **d)** HIP 22632 with $T_{\rm eff}$/ log g/[Fe/H]/log(Be/H) = 5825/4.30/−1.40/−12.17, dashed line, vs. HIP 53070 with $T_{\rm eff}$/ log g/[Fe/H]/log(Be/H) = 5900/4.20 /−1.40/−11.80, solid line.

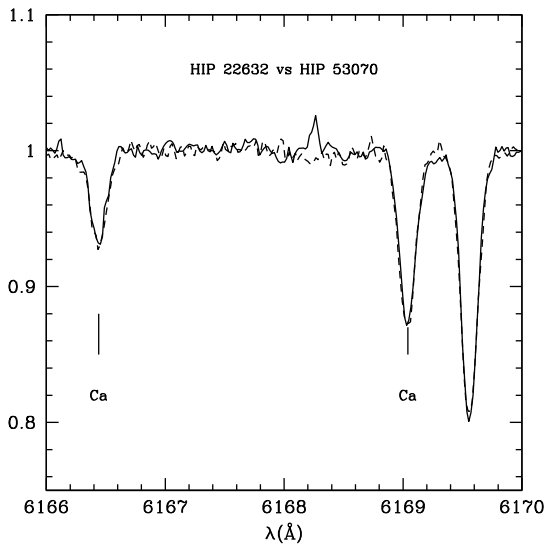

Fig. 15. Comparison between two calcium lines in the spectra of stars HIP 22632 (dashed line) and HIP 53070 (solid line). The Be region of these stars is shown in the last panel of the previous Figure. The stars have similar metallicity, similar atmospheric parameters, and similar abundances of α-elements but different Be abundances.

the subsample of possible binaries and the other stars is found. Binaries therefore do not seem to be responsible for the observed scatter.

7.1.3. The F00 subsample

As discussed in Sect. 3.2 there is a systematic difference in temperature and [Fe/H] between the results of Edvardsson et al. (1993) and Fulbright (2000), although within the uncertainties. This difference in metallicity may introduce some scatter into the relations shown in Figs. 10 and 11. In the final sample of 73 stars, 49 have parameters calculated by F00, of which 26 are halo stars and 19 are thick-disk stars. We repeated the analysis with this subsample of stars. The linear fits using only the Fullbright stars and rms are statistically identical to the ones obtained with the whole clean sample (also listed in Table 9). The equivalent of Figs. 10 and 11 for the F00 subsample are given in Appendix B.

7.2. log(Be/H) vs. [Fe/Be]

The evolution of a given element in the Galaxy is usually analyzed in a plot of [Element/Fe] vs. [Fe/H]. If Be is a better time scale than Fe, then changing Fe for Be in this kind of discussion would be the natural follow-up. In Fig. 16 we plot [Fe/Be] as a function of log(Be/H).

A decrease in [Fe/Be] with increasing log(Be/H) is seen. It is interesting to see that for log(Be/H) > −11.5 the majority of the stars have a sub-solar Fe/Be ratio. In principle similar plots could be constructed also for elements other that iron.

8. Be as a chronometer

The hypothesis that Be can be used as an age indicator relies on assumptions about the uniformity of the GCR in the early-Galaxy. This uniformity is necessary to assure the Be clock runs at a uniform pace within the relevant region of the Galaxy. In

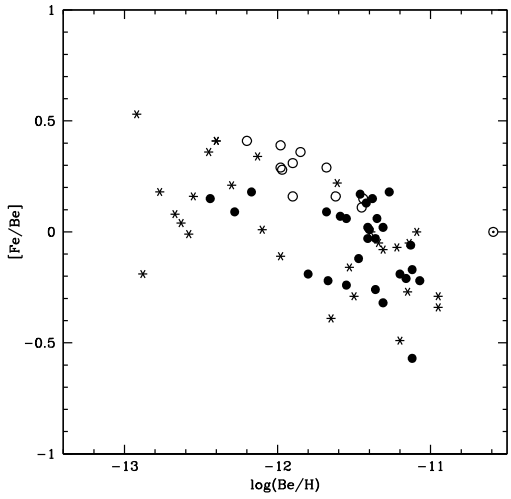

Fig. 16. Diagram of log(Be/H) vs. [Fe/Be]. Thick disk stars are shown as filled circles, halo stars as starred symbols, and the subgroup of "Fe-rich" halo stars discussed Sect. 8 is shown as open circles.

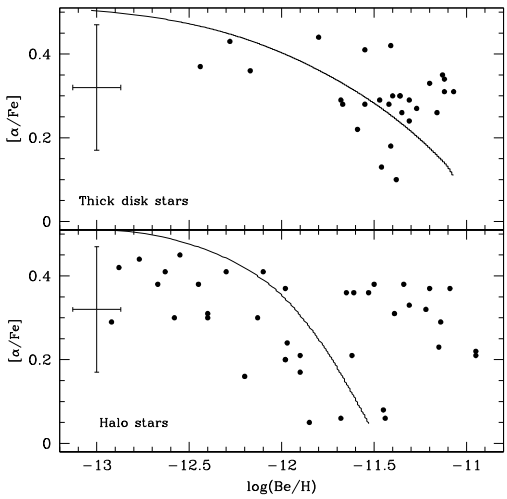

Fig. 17. Diagram of [α/Fe] vs. log(Be/H). The thick-disk stars are shown in the *upper panel*, while the halo stars are shown in the *lower panel*. The thick-disk stars diagram is characterized by a large scatter, while the halo stars diagram clearly divides into two sequences. The curves are the predictions of the models by Valle et al. (2002).

general, models of Galactic chemical evolution do not include a detailed treatment of GCR propagation and confinement. The model we use to compare with our observations (see Valle et al. 2002, and references therein) follows a multizone treatment of the Galaxy, where each component is characterized by different star formation rates with a radial dependence. The GCR, however, has neither radial nor vertical dependence. The interpretation of the results in light of these models may, therefore, be somewhat limited.

Pasquini et al. (2005) began using the Be abundances as a time scale, and show that halo and thick-disk stars separate in a diagram of log(Be/H) vs. [α/Fe]. Their sample, however, is composed of only twenty stars analyzed by Boesgaard et al. (1999). In a diagram [O/Fe] vs. log(Be/H), the beryllium abundance in the abscissa can be considered as "increasing time" while the [O/Fe] ratio in the ordinate can be considered as the "star formation rate" (SFR). We use [α/Fe] here rather than [O/Fe]. In Fig. 17 we show the [α/Fe] vs. log(Be/H) for our sample. The figure is divided into two panels; in the upper panel we plot the thick disk stars and in the lower panel we plot the halo stars. In the same figure the two models from Pasquini et al. (2005), derived from Valle et al. (2002), are also shown. In Fig. 18 we show the classical [α/Fe] vs. [Fe/H] diagram, also divided with the thick-disk stars in the upper panel and the halo stars in the lower panel.

From Fig. 17 it appears that the model is fairly successful in reproducing the general trend of the thick-disk stars. However the halo stars appear to split along a double sequence. The most striking is the group of stars with high [α/Fe] and high log(Be/H), which the model totally fails to reproduce. From the point of view of α elements and beryllium abundance, this group of stars is essentially indistinguishable from the thick-disk stars.

The first conclusion that may be drawn from this plot is that the thick disk appears to be a fairly homogeneous population, where the "Be chronometer" may be used with some confidence. The halo instead appears to be more complex. In the following sections we discuss the use of Be as a chronometer in the two populations separately. Galactic orbits for the majority of the sample stars were computed by Gratton et al. (2003a). For the few remaining stars, new orbits were calculated following the same method. We refer to Gratton et al. (2003a) for the details. The orbital parameters are listed in Table 6. In Figs. 19 and 20 we show the correlation of chemical and dynamical properties. Alternative to the halo – thick disk distinction, we could have used the accretion – dissipative component distinction introduced by Gratton et al. (2003a,b). We refer to the original papers for a detailed presentation of the kinematic criteria used for this division. We did this exercise, and the main conclusions are essentially the same. The corresponding plots are provided in Appendix C.

8.1. The Be chronometer in the thick disk

Thick-disk stars show smaller scatter in all diagrams, and it seems possible to understand their formation in a relatively simple way. The most interesting feature is, however, the anticorrelation of [α/Fe] with $R_{\rm min}$ in our sample (Fig. 20). At first glance, this anticorrelation seems to be driven by the two stars with largest $R_{\rm min}$. However, even when restricting the sample to stars with $R_{\rm min} < 6$ kpc, the probability of correlation is 99.8%. A similar anticorrelation is also present in the data of Gratton et al. (2003b, see their Fig. 6). If $R_{\rm min}$ is representative of the radius of formation of a star, neglecting the phenomena of orbital diffusion, then the simplest interpretation is that the thick disk experienced a higher SFR in the inner regions than in the outer regions. This does not contrast with the notion that the thick is very old and massive (Fuhrmann 1998, 2000, 2004, 2008). In fact the star formation is supposed to have continued for about 2 Gyr (Fuhrmann 2004), which is ample time for the external regions experiencing a low SFR to develop a lower α/Fe than the inner regions where the SFR was higher. Note also that the most Be-poor, i.e. oldest, stars are found at low $R_{\rm min}$. The emerging picture is that of a dissipative thick disk formed inside-out.

Such an anticorrelation is not present in the log(Be/H) vs. $R_{\rm min}$ plot, as shown in the upper panel of Fig. 20. It is also not present in the [Be/Fe] vs. $R_{\rm min}$ plot. This lack of anticorrelation is an important result. The major objection to the use of Be as a time indicator is the possibility that the abundance of this element is dominated by local events rather than by the relativistic component. The log(Be/H) vs. $R_{\rm min}$ diagram does not show

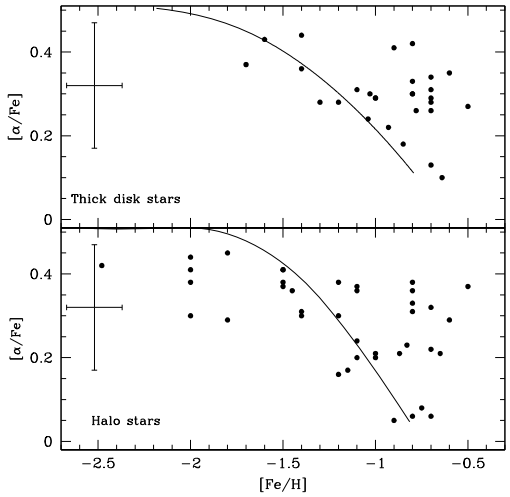

Fig. 18. Diagram of [α/Fe] vs. [Fe/H]. The thick-disk stars are shown in the *upper panel*, while the halo stars are shown in the *lower panel*. The curves are the predictions of the models by Valle et al. (2002).

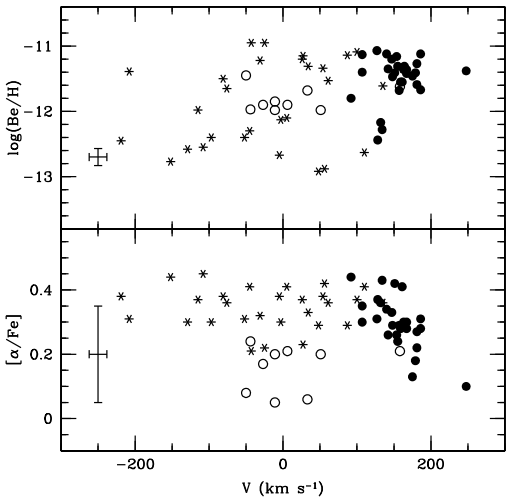

Fig. 19. Diagram of log(Be/H) vs. the V, the component of the space velocity of the star in the direction of the disk rotation. The thick-disk stars are shown as filled circles, halo stars are shown as starred symbols, and the subgroup of halo stars as open circles. A typical error of $\pm$12 km s^{-1} in V was adopted (see Gratton et al. 2003b).

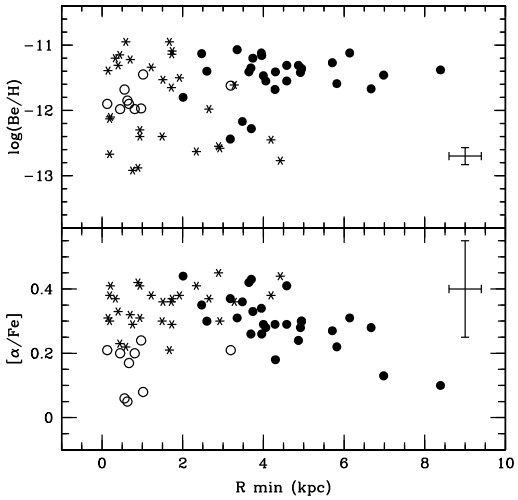

Fig. 20. Diagram of log(Be/H) vs. $R_{\rm min}$, the perigalactic distance of the stellar orbit. The thick disk stars are shown as filled circles, halo stars are shown as starred symbols, and the subgroup of halo stars as open circles. A typical error of $\pm$0.40 Kpc in $R_{\rm min}$ was adopted (see Gratton et al. 2003b).

evidence of a general decrease in Be with the distance from the galactic center, as could be expected if the local flux of GCR was the dominant factor.

The range in Be covered by the thick-disk stars of our sample is relatively small. Moreover, most of the Be-poor stars are present at a relatively small $R_{\rm min}$. This agrees with the notion of a rather fast formation for the thick disk (Fuhrmann 2004, 2008). As a reference time scale, the reader may consider that the thick-disk models shown in the upper panel of Fig. 17 have a star formation period of 1 Gyr.

8.2. The Be chronometer in the halo

For a long time the debate on the halo formation was centered on the opposite views of "monolithic collapse" (Eggen et al. 1962) and "fragment assembly" (Searle & Zinn 1978). It is now understood that these represent rather idealized extreme cases that do not happen in reality. Major insights into halo assembly have come from simulations of galaxy formation in a cosmological context (see e.g. Font et al. 2006, and references therein). In these simulations in the ΛCDM scenario, the galaxy formation proceeds hierarchically, nevertheless they predict the existence of metallicity gradients and other features typical of the "monolithic collapse". In light of these simulations, we should expect to find, in a halo sample, stars that have been accreted from many dwarf satellite galaxies, as well as stars formed on short time scales in the halo (i.e. a "monolithic collapse"-like component).

Even before considering our data one can expect that the "Be chronometer" was running at a different pace in the different components out of which the halo was assembled. This in fact appears quite obvious from Fig. 17. The stars with high Be abundances and high [α/Fe] cannot be reproduced by our model. It is tempting to interpret these stars as "accreted" from satellites in which the Be production was more efficient than in the Milky Way. However, these stars do not display any peculiar kinematic property.

The good news is that the halo stars do not fill uniformly the log(Be/H) – [α/Fe] plane, but position around only two, rather well-defined sequences. This means that there is some prospect for also using the "Be chronometer" for the halo stars. Hopefully future models will be able to explain the two sequences and calibrate the Be abundance versus time. By use of a diagram like Fig. 17, one should be able to decide which sequence any given star belongs to.

The reality of the separation seen in Fig. 17 is dependent on the error of the abundances. A statistical test shows that the halo stars in the top right of panel b in this figure have probabilities between 40% to 9% of following the model curve. This suggests that the separation seen in the figure is real. These probabilities are likely to improve, and more stringent constraints might be derived, when oxygen, which is a pure SN II product, is determined in a homogeneous way for all the sample stars (Smiljanic et al., in preparation).

In Figs. 19 and 20 we plot both [α/Fe] and log(Be/H) as a function of V, the spatial velocity in the direction of the

rotation of Galaxy, and R_{min}, the perigalactic distance, respectively. At the end of the ′90s, several halo stars with a low [α/Fe] were identified (Carney et al. 1997; Nissen & Schuster 1997) and were considered as "accreted" objects. Inspection of Fig. 17 shows that such stars are however predicted by our evolutionary model. To easily identify the "low α" stars (which we define as stars with [α/Fe] ≤ 0.25 and log(Be/H) ≤ -11.4) in the figures, we plot them as open circles. These stars have very similar kinematic properties. They tend to have V close to zero and $R_{min} \leq 1$ kpc, although the statistics are too few to allow a robust claim. They seem to be a group of non-rotating stars going very close to the Galactic center, a behavior that might be expected to be shown by accreted stars that sink to the Galactic center by dynamical friction. They also show a remarkably narrow range of Be abundances, suggesting a narrow range in age for this component. These characteristics might hint at a possible common origin for these stars.

A robust interpretation of these components in light of our evolutionary model does not seem possible. Unlike what is assumed by the model, our results suggest that the halo is not a single uniform population where a clear age-metallicity relation can be defined. The splitting of the halo into the two components identified in this work might be related to the accretion of external components or simply to variations in the star formation in different and initially independent regions of the early halo.

9. Summary

We have presented the largest sample, to date, of Be abundances in stars. We confirm the existence of a linear increase in Be with [Fe/H] and [α/H], as has been found by all the previous investigations. However, thanks to the large dimension of our sample and the homogeneous analysis, we have a marginal detection of an excess scatter in the log(Be/H) – [Fe/H] relation, above what may be expected by observational errors. A similar scatter is not obvious in the log(Be/H) – [α/H] relation, although we identify a pair of stars with similar parameters and similar [α/H] but with a 0.4 dex difference in Be abundance. Our interpretation of this scatter is that it arises from the different evolutionary time scales of different Galactic components (halo, thick disk). Beryllium is a good indicator of time, anywhere, but metal enrichment proceeds at a different pace in different environments.

We tested the use of Be as a chronometer by comparing our observations to model predictions. The result appears to be fairly satisfactory for the thick disk, which we confirm to be a homogeneous population. There appears to be no trend in Be abundance with perigalactic distance. We take this as evidence that the Be production is dominated by the relativistic component of the cosmic rays and largely insensitive to local events. Our models of Be evolution, however, fail to reproduce the observations for a subset of halo stars. More sophisticated models that explicitly consider the merger history of the halo should be envisaged. In a plot of log(Be/H) versus [α/Fe] (Fig. 17), the halo stars do not fill the plane randomly, but align in two rather clearly defined sequences. Only one of these two sequences can be explained by our models. However, most stars of this same component show very similar kinematics and a narrow range in Be (age). They seem to be a group of non-rotating stars going very close to the Galactic center so might have a common origin.

For the halo stars we do not identify any significant correlation between chemical and kinematic properties. For the thick disk, instead, we find a significant anticorrelation of [α/Fe] with perigalactic distance. This anticorrelation might be interpreted as evidence that the SFR was lower in the outer regions of the thick disk, pointing towards an inside-out formation.

Even though not all our observations can be readily interpreted in terms of existing models, we believe that our study has highlighted the usefulness of Be abundance in studying the different Galactic populations.

Acknowledgements. This work was developed during the visit of R.S. to ESO made possible by a CAPES fellowship (1521/06-3) and support from the ESO DGDF. R.S. acknowledges an FAPESP Ph.D. fellowship (04/13667-4). P.B. acknowledges support from EU contract MEXT-CT-2004-014265 (CIFIST). D. G. acknowledges support from EC grant MRTN-CT-2006-035890-Constellation. We thank Francesca Primas for making her line list available and for her much appreciated help in analyzing the spectra.

References

Andersen, J., Gustafsson, B., & Lambert, D. L. 1984, A&A, 136, 65
Asplund, M. 2004, A&A, 417, 769
Bagnulo, S., Jehin, E., Ledoux, C., et al. 2003, Messenger, 114, 10
Balachandran, S. C., & Bell, R. A. 1998, Nature, 392, 791
Barbuy, B., Perrin, M.-N., Katz, D., Coelho, P., et al. 2003, A&A, 404, 661
Beckman, J. E., Abia, C., & Rebolo, R. 1989, Ap&SS, 157, 41
Beers, T. C., Suzuki, T. K., & Yoshii, Y. 2000, in The Light Elements and their Evolution, ed. L. da Silva, J. R. de Medeiros, & M. Spite, IAU Symp., 198, 425
Boesgaard, A. M. 2007, ApJ, 667, 1196
Boesgaard, A. M., & Tripicco, M. J. 1986, ApJ, 302, L49
Boesgaard, A. M., & King, J. R. 1993, AJ, 106, 2309
Boesgaard, A. M., & King, J. R. 2002, ApJ, 565, 587
Boesgaard, A. M., & Novicki, M. 2006, ApJ, 641, 1122
Boesgaard, A. M., Deliyannis, C. P., King, J. R., et al. 1999, AJ, 117, 1549
Boesgaard, A. M., Armengaud, E., King, J. R., Deliyannis, C. P., & Stephens, A. 2004, ApJ, 613, 1202
Boesgaard, A. M., Stephens, A., & Deliyannis, C. P. 2005, ApJ, 633, 398
Bonifacio, P., & Molaro, P. 1997, MNRAS, 285, 847
Bonifacio, P., Molaro, P., Sivarani, T., et al. 2007, A&A, 462, 851
Caffau, E., Bonifacio, P., Faraggiana, R., et al. 2005, A&A, 441, 533
Carney, B. W., Latham, D. W., Laird, J. B., Grant, C. E., & Morse, J. A., 2001, AJ, 122, 3419
Carney, B. W., Wright, J. S., Sneden, C., et al. 1997, AJ, 114, 363
Cassé, M., Lehoucq, R., & Vangioni-Flam, E. 1995, Nature, 373, 318
Castelli, F., & Kurucz, R. L. 2003, in Proc. IAU Symp., 210, A20
Castelli, F., Gratton, R. G., & Kurucz, R. L. 1997, A&A, 318, 841
Castilho, B. V., Spite, M., Barbuy, B., et al. 1999, A&A, 345, 249
Charbonnel, C., & Talon, S. 1999, A&A, 351, 635
Charbonnel, C., & Primas, F. 2005, A&A, 442, 961
Chen, Y. Q., Nissen, P., Benoni, T., & Zhao, G. 2001, A&A, 371, 943
Chmielewski, Y., Müller, E. A., & Brault, J. W. 1975, A&A, 42, 37
Coelho, P., Barbuy, B., Meléndez, J., Schiavon, R. P., & Castilho, B. V. 2005, A&A, 443, 735
Dekker, H., D'Odorico, S., Kaufer, A., Delabre, B., & Kotzlowski, H. 2000, SPIE, 4008, 534
Dommanget, J., & Nys, O. 1994, Com. de l'Observ. Royal de Belgique, 115, 1
Duncan, D. K., Lambert, D. L., & Lemke, M. 1992, ApJ, 401, 584
Edvardsson, B., Andersen, J., & Gustafsson, B. 1993, A&A, 275, 101
Eggen, O. J., Lynden-Bell, D., & Sandage, A. R. 1962, ApJ, 136, 748
ESA 1997, The Hipparcos and Tycho catalogues, ESA SP-1200
Favata, F., Micela, G., & Sciortino, S. 1996, A&A, 311, 951
Fields, B. D., & Olive, K. A. 1999, ApJ, 516, 797
Fouts, G. 1987, PASP, 99, 986
Font, A. S., Johnston, K. V., Bullock, J. S., & Robertson, B. E. 2006, ApJ, 638, 585
Fuhrmann, K. 1998, A&A, 338, 161
Fuhrmann, K. 2000, http://www.ing.iac.es/~klaus/
Fuhrmann, K. 2004, Astron. Nachr., 325, 3
Fuhrmann, K. 2008, MNRAS, 384, 173
Fulbright, J. P. 2000, AJ, 120, 1841
Garcia Lopez, R. J., Rebolo, R., & Perez de Taoro, M. R. 1995, A&A, 302, 184
Garcia Lopez, R. J., Severino, G., & Gomez, M. T. 1995, A&A, 297, 787
García Pérez, A. E., & Primas, F. 2006, A&A, 447, 299
Gilmore, G., Gustafsson, B., Edvardsson, B., & Nissen, P. E. 1992, Nature, 357, 379
Gliese, W., & Jahreiss, H. 1988, Ap&SS, 14, 49
Goldberg, D., Mazeh, T., Latham, D. W., et al. 2002, AJ, 124, 1132

Gratton, R. G., & Sneden, C. 1988, A&A, 204, 193
Gratton, R. G., & Sneden, C. 1991, A&A, 241, 501
Gratton, R. G., Sneden, C., Carretta, E., & Bragaglia, A. 2000, A&A, 354, 169
Gratton, R. G., Carretta, E., Desidera, S., et al. 2003a, A&A, 404, 187
Gratton, R. G., Carretta, E., Desidera, S., et al. 2003b, A&A, 406, 131
King, J. R. 2001, AJ, 122, 3115
King, J. R. 2002, PASP, 114, 25
Korn, A. J., Grundahl, F., Richard, O., et al. 2007, ApJ, 671, 402
Kurucz, R. L., Furelind, I., Brault, J., & Testerman, L. 1984, Solar Flux Atlas from 296 to 1300 nm, NOAO Atlas, No. 1
Latham, D. W., Stefanik, R. P., Torres, G., et al. 2002, AJ, 124, 1144
Lindgren, H., & Ardeberg, A. 1996, A&AS, 119, 25
Lodders, K. 2003, ApJ, 591, 1220
Lu, P. K., Demarque, P., van Altena, W., McAlister, H., & Hartkopf, W. 1987, AJ, 94, 1318
McAlister, H. A., Hartkopf, W. I., Hutter, D. J., Shara, M. M., & Franz, O. G. 1987, AJ, 93, 183
MacConnell, D. J., Osborn, W. H., & Miller, R. J. 1997, AJ, 114, 1268
McWilliam, A., Preston, G. W., Sneden, C., & Searle, L. 1995, AJ, 109, 2757
Meléndez, J., Barbuy, B., Bica, E., et al. 2003, A&A, 411, 417
Meneguzzi, M., & Reeves, H. 1975, A&A, 40, 99
Meneguzzi, M., Audouze, J., & Reeves, H. 1971, A&A, 15, 337
Molaro, P., & Beckaman, J. 1984, A&A, 139, 394
Molaro, P., Bonifacio, P., Castelli, F., & Pasquini, L. 1997a, A&A, 319, 593
Molaro, P., Bonifacio, P., & Pasquini, L. 1997b, MNRAS, 292, L1
Nissen, P. E., & Schuster, W. J. 1997, A&A, 326, 751
Nordström, B., Mayor, M., Andersen, J., et al. 2004, A&A, 418, 989
Parizot, E. 2000, A&A, 362, 786
Parizot, E., & Drury, L. 2000, A&A, 356, L66
Pasquini, L., Bonifacio, P., Randich, S., Galli, D., & Gratton, R. G. 2004, A&A, 426, 651
Pasquini, L., Galli, D., Gratton, R. G., et al. 2005, A&A, 436, L57
Pasquini, L., Bonifacio, P., Randich, S., et al. 2007, A&A, 464, 601
Patience, J., White, R. J., Ghez, A. M., et al. 2002, ApJ, 581, 654
Piau, L., Beers, T. C., Balsara, D. S., et al. 2006, ApJ, 653, 300
Prantzos, N., Casse, M., & Vangioni-Flam, E. 1993, ApJ, 403, 630
Primas, F., Duncan, D. K., Pinsonneault, M. H., Deliyannis, C. P., & Thorburn, J. A. 1997, ApJ, 480, 784
Primas, F., Asplund, M., Nissen, P. E., & Hill, V. 2000a, A&A, 364, L42
Primas, F., Molaro, P., Bonifacio, P., & Hill, V. 2000b, A&A, 362, 666
Prochaska, J. X., Naumov, S. O., Carney, B. W., McWilliam, A., & Wolfe, A. M. 2000, AJ, 120, 2513
Randich, S., Primas, F., Pasquini, L., & Pallavicini, R. 2002, A&A, 387, 222
Randich, S., Primas, F., Pasquini, L., Sestito, P., & Pallavicini, R. 2007, A&A, 469, 163
Rebolo, R., Abia, C., Beckman, J. E., & Molaro, P. 1988, A&A, 193, 193
Reeves, H., Fowler, W. A., & Hoyle, F. 1970, Nature, 226, 727
Romano, D., Matteucci, F., Molaro, P., & Bonifacio, P. 1999, A&A, 352, 117
Ryan, S. G., & Deliyannis, C. P. 1995, ApJ, 453, 819
Ryan, S. G., Bessel, M., Sutherland, R. S., & Norris, J. E. 1990, ApJ, 348, 57
Ryan, S. G., Norris, J. E., Bessel, M. S., & Deliyannis, C. 1992, ApJ, 388, 184
Ryan, S. G., Beers, T. C., Kajino, T., & Rosolankova, K. 2001, ApJ, 547, 231
Santos, N. C., Garcia Lopez, R. J., Israelian, G., et al. 2002, A&A, 386, 1028
Santos, N. C., Israelian, G., Randich, S., García López, R. J., & Rebolo, R. 2004, A&A, 425, 1013
Searle, L., & Zinn, R. 1978, ApJ, 225, 357
Smiljanic, R., & Barbuy, B. 2007, in Proc. IAU Symp. 241, ed. A. Vazdekis, & R. F. Peletier, 103
Smiljanic, R., Pasquini, L., & Primas, F., et al. 2008, MNRAS, 385, L93
Spite, F., & Spite, M. 1982, A&A, 115, 357
Spite, M., Maillard, J. P., & Spite, F. 1984, A&A, 141, 56
Spite, M., Pasquini, L., & Spite, F. 1994, A&A, 290, 217
Stephens, A., & Boesgaard, A. M. 2002, AJ, 123, 1647
Stephens, A., Boesgaard, A. M., King, J. R., & Deliyannis, C. P. 1997, ApJ, 491, 339
Stryker, L. L., Hesser, J. E., Hill, G., Garlick, G. S., & O'Keefe, L. M. 1985, PASP, 97, 247
Suzuki, T. K., & Yoshii, Y. 2001, ApJ, 549, 303
Suzuki, T. K., Yoshii, Y., & Kajino, T. 1999, ApJ, 522, L125
Takeda, Y., & Kawanomoto, S. 2005, PASJ, 57, 45
Thomas, D., Schramm, D. N., Olive, K. A., & Fields, B. D. 1993, ApJ, 406, 569
Thorburn, J. A., & Hobbs, L. M. 1996, AJ, 111, 2106
Travaglio, C., Randich, S., Galli, D., et al. 2001, ApJ, 559, 909
Valle, G., Ferrini, F., Galli, D., & Shore, S. N. 2002, ApJ, 566, 252
Vangioni-Flam, E., Audouze, J., Oberto, Y., & Casse, M. 1990, ApJ, 364, 568
Vangioni-Flam, E., Ramaty, R., Olive, K. A., & Cassé, M. 1998, A&A, 337, 714
Venn, K. A., Irwin, M., Shetrone, M. D., et al. 2004, AJ, 128, 1177
Wallerstein, G., Herbig, G. H., & Conti, P. S. 1965, ApJ, 141, 610

Table 1. Data of the sample stars.

HIP	HD	Other name	V mag	π mas	σ_π mas	M_V mag	BC mag	M_{bol} mag	log $(L_\star/L_\odot)$	binary?
171	224 930	85 Peg A	5.75	80.63	3.03	5.28	−0.27	5.02	−0.11	ABCD[1]
3026	3567	–	9.26	9.57	1.38	4.16	−0.16	4.00	+0.30	no[2]
7459	–	CD-61 0282	10.10	11.63	1.19	5.43	−0.16	5.27	−0.21	–
10 140	–	G 74-5	8.77	17.66	1.29	5.00	−0.22	4.78	−0.01	ABCD[1]
10 449	–	G 159-50	9.09	16.17	1.34	5.13	−0.20	4.93	−0.07	no[2]
11 952	16 031	–	9.77	8.67	1.81	4.46	−0.18	4.28	+0.19	Susp.[3]
13 366	17 820	–	8.38	15.38	1.39	4.31	−0.16	4.15	+0.24	no[4]
14 086	18 907	ϵ For	5.89	32.94	0.72	3.48	−0.33	3.15	+0.64	yes[5]
14 594	19 445	–	8.06	25.85	1.14	5.12	−0.23	4.89	−0.06	no[6]
17 001	–	CD-24 1782	9.92	4.42	1.75	–	–	–	–	–
17 147	22 879	G 80-15	6.70	41.07	0.86	4.77	−0.17	4.60	+0.06	no[2]
18 802	25 704	–	8.10	19.02	0.87	4.50	−0.15	4.35	+0.16	AB[1]
19 007	25 673	–	9.56	24.23	1.53	6.48	−0.26	6.23	−0.59	–
19 814	–	G 82-5	10.60	24.27	23.10	–	−0.25	–	–	no[2]
21 609	29 907	–	9.85	17.00	0.98	6.00	−0.28	5.72	−0.39	AB[7]
22 632	31 128	–	9.13	15.55	1.20	5.09	−0.21	4.88	−0.05	no[4]
24 030	241 253	G 84-37	9.72	10.29	1.66	4.78	−0.19	4.60	+0.06	no[2]
24 316	34 328	–	9.44	14.55	1.01	5.25	−0.21	5.04	−0.12	–
31 188	46 341	–	8.62	16.86	0.98	4.75	−0.16	4.59	+0.06	–
31 639	–	CD-25 3416	9.65	17.59	1.34	5.88	−0.25	5.63	−0.35	–
33 221	–	CD-33 3337	9.03	9.11	1.01	3.83	−0.17	3.66	+0.44	–
33 582	51 754	–	9.05	14.63	1.39	4.88	−0.16	4.72	+0.01	no[2]
34 285	–	CD-57 1633	9.54	10.68	0.91	4.68	−0.16	4.52	+0.09	no[4]
36 491	59 374	G 88-31	8.50	20.00	1.66	5.01	−0.17	4.84	−0.03	no[2]
36 640	59 984	HR 2883	5.90	33.40	0.93	3.52	–	–	–	AB[1]
36 818	–	CD-45 3283	10.43	15.32	1.38	6.36	−0.19	6.17	−0.57	–
36 849	60 319	G 88-40	8.95	12.15	1.24	4.37	−0.17	4.20	+0.22	no[2]
37 853	63 077	HR 3018	5.36	65.79	0.56	4.46	−0.15	4.31	+0.18	wide[8]
38 625	64 606	G 112-54	7.44	52.01	1.85	6.02	−0.25	5.77	−0.41	yes[2]
42 124	–	G 114-26	9.69	12.37	1.72	5.15	–	–	–	yes[9]
45 592	74 000	–	9.66	7.26	1.32	3.96	−0.21	3.76	+0.40	no[2]
44 075	76 932	HR 3578	5.86	46.90	0.97	4.22	−0.14	4.08	+0.27	yes[4]
44 124	–	G 114-26	9.69	12.37	1.72	5.15	–	–	–	yes[9]
45 554	–	G 46-31	10.86	3.79	2.16	3.75	−0.15	3.60	+0.46	yes[2]
48 152	84 937	–	8.31	12.44	1.06	3.78	−0.19	3.59	+0.46	no[10]
50 139	88 725	–	7.74	27.67	1.01	4.95	−0.19	4.76	0.00	no[2]
52 771	–	BD+29 2091	10.24	10.55	1.75	5.36	−0.21	5.15	−0.16	Susp.[11]
53 070	94 028	G 58-25	8.23	19.23	1.13	4.65	−0.18	4.47	+0.11	no[2]
55 022	97 916	–	9.21	7.69	1.23	3.64	−0.10	3.54	+0.48	yes[10]
57 265	–	G 121-12	10.37	6.14	1.82	4.31	−0.19	4.12	+0.25	no[2]
58 145	–	BD-21 3420	10.15	5.43	1.44	3.82	−0.16	3.66	0.43	–
58 962	105 004	–	10.21	2.68	4.49	–	−0.17	–	–	ABC[1]
59 490	106 038	G 12-21	10.18	9.16	1.50	4.99	−0.16	4.83	−0.03	no[2]
59 750	106 516	HR 4657	6.11	44.34	1.01	4.34	−0.11	4.23	+0.21	AB[1]
60 632	108 177	G 13-35	9.67			4.87	−0.17	4.70	+0.02	no[2]
62 882	111 980	–	8.38	12.48	1.38	3.86	–	–	–	AB[1]
63 559	113 083	–	8.05	18.51	1.12	4.39	−0.18	4.21	+0.22	yes[4]
63 918	113 679	–	9.70	6.82	1.32	3.87	−0.16	3.71	+0.42	no[4]
64 426	114 762	–	7.31	24.65	1.44	4.27	−0.16	4.11	+0.26	yes[12]
66 665	–	BD+13 2698	9.37	7.44	1.70	3.73	−0.20	3.53	+0.49	no[2]
67 655	120 559	–	7.97	40.02	1.00	5.98	−0.26	5.72	−0.39	–
67 863	121 004	–	9.04	16.73	1.35	5.16	−0.16	5.00	−0.10	no[4]
70 681	126 681	–	9.33	19.16	1.44	5.74	−0.22	5.52	−0.31	no[4]
71 458	128 279	–	7.97	5.96	1.32	–	–	–	–	no[4]
72 461	–	BD+26 2606	9.74	10.28	1.42	4.80	−0.21	4.59	+0.06	yes[11]
74 067	134 088	–	8.00	28.29	1.04	5.26	−0.20	5.06	−0.12	no[4]
74 079	134 169	–	7.68	16.80	1.11	3.81	−0.16	3.65	+0.44	yes[4]
77 946	142 575	–	8.61	6.56	1.23	2.69	−0.11	2.58	+0.87	–
80 003	–	G 168-42	11.51	9.12	3.01	6.31	−0.21	6.10	−0.54	yes[2]
80 837	148 816	G 17-21	7.28	24.34	0.90	4.21	−0.17	4.04	+0.28	no[2]
81 170	149 414	–	9.63	20.71	1.50	6.21	−0.26	5.95	−0.48	ABCDE[1]
85 963	159 307	–	7.41	13.40	0.99	3.05	−0.13	2.92	+0.73	yes[4]
87 693	–	BD+20 3603	9.71	6.47	7.85	3.76	−0.19	3.58	+0.47	yes[4]

Table 1. continued.

HIP	HD	Other name	V mag	π mas	σ_π mas	M_V mag	BC mag	M_{bol} mag	log $(L_\star/L_\odot)$	binary?
88 010	163 810	–	9.63	11.88	2.21	5.00	−0.28	4.72	+0.01	AB[1]
92 781	175 179	–	9.08	11.55	1.81	4.45	−0.16	4.29	+0.18	no[2]
94 449	179 626	–	9.17	7.52	1.36	3.55	−0.21	3.34	+0.56	no[2]
98 020	188 510	–	8.83	25.32	1.17	5.85	−0.27	5.58	−0.33	yes[4]
98 532	189 558	–	7.72	14.76	1.10	3.57	–	–	–	AB[4]
100 568	193 901	–	8.65	22.88	1.24	5.45	−0.19	5.26	−0.20	no[2]
100 792	194 598	G 24-15	8.36	17.94	1.24	4.63	−0.17	4.46	+0.12	no[2]
101 346	195 633	–	8.53	8.63	1.16	3.21	−0.13	3.08	+0.67	no[4]
103 498	199 289	–	8.29	18.94	1.03	4.68	−0.17	4.51	+0.10	no[4]
104 660	201 889	–	8.04	17.95	1.44	4.31	−0.20	4.11	+0.26	AB[1]
105 858	203 608	HR 8181	4.22	108.50	0.59	4.40	−0.13	4.27	+0.19	no[4]
105 888	204 155	G 25-29	9.03	13.02	1.11	4.07	−0.16	3.91	+0.33	no[2]
106 447	–	G 26-12	12.15	−1.57	4.54	–	−0.21	–	–	no[2]
107 975	207 978	15 Peg	5.54	36.15	0.69	3.32	−0.11	3.21	+0.62	no[13]
108 490	208 906	–	6.95	34.12	0.70	4.62	−0.15	4.47	+0.11	AB[1]
109 067	–	G 18-28	9.55	21.52	1.59	6.21	−0.26	5.96	−0.48	AB[2]
109 558	–	G 126-62	9.47	8.43	1.42	4.10	−0.18	3.92	+0.33	AB[2]
109 646	210 752	–	7.40	26.57	0.85	4.44	−0.14	4.30	+0.18	no[4]
112 229	215 257	G 27-44	7.40	23.66	0.97	4.14	−0.14	4.14	+0.25	no[2]
114 271	218 502	–	8.50	14.33	1.20	4.28	−0.11	4.17	+0.26	–
114 962	219 617	G 273-1	8.17	12.04	2.41	3.57	−0.20	3.37	+0.55	ABCD[1]
115 167	–	G 29-23	10.21	3.26	2.20	2.78	−0.20	2.58	+0.87	AB[1]
117 041	222 766	–	10.15	8.46	1.76	4.79	−0.26	4.53	+0.09	no[6]
–	–	G05-19	11.12	–	–	–	−0.16	–	–	no[2]
–	–	G05-40	10.79	–	–	–	−0.17	–	–	no[2]
–	–	G66-51	10.63	–	–	–	−0.26	–	–	no[2]
–	–	G166-37	12.66	5.20[14]	0.70	6.24	− 0.27	5.97	−0.49	no[2]
–	–	G170-21	12.51	–	–	–	−0.21	–	–	no[2]

[1] Dommanget & Nys (1994); [2] Latham et al. (2002); [3] Fouts (1987); [4] Nordström et al. (2004); [5] this work; [6] Lu et al. (1987); [7] Lindgren & Ardeberg (1996); [8] Gliese & Jahreiss (1988); [9] Goldberg et al. (2002); [10] Carney et al. (2001); [11] Stryker et al. (1985); [12] Patience et al (2002); [13] McAlister et al. (1987); [14] MacConnell et al. (1997).

Table 2. Log book of the observations.

HIP	Date of obs.	Type[1]	Exp. time (s)	R	λ_c (Å)	S/N^2 (final)
171	13.Oct.2005	New UVES	2×150	35 000	3460	100
	13.Oct.2005	New UVES	2×30		5800	
	13.Oct.2005	New UVES	2×30		8600	
3026	08.Oct.2001	Archive	4200	35 000	3460	130
7459	22.Sep.2005	New UVES	2×1800	35 000	3460	60
	22.Sep.2005	New UVES	2×800		5800	
	22.Sep.2005	New UVES	2×800		8600	
10 140	14.Oct.2005	New UVES	2×900	35 000	3460	70
	14.Oct.2005	New UVES	2×350		5800	
	14.Oct.2005	New UVES	2×350		8600	
10 449	14.Oct.2005	New UVES	2×900	35 000	3460	90
	14.Oct.2005	New UVES	2×350		5800	
	14.Oct.2005	New UVES	2×350		8600	
11 952	13.Oct.2005	New UVES	1500	35 000	3460	75
	13.Oct.2005	New UVES	2×650		8600	
13 366	13.Oct.2005	New UVES	450 and 900	35 000	3460	90
	13.Oct.2005	New UVES	2×150		5800	
	13.Oct.2005	New UVES	2×700		8600	
14 086	23.Sep.2005	New UVES	2×150	35 000	3460	70
	23.Sep.2005	New UVES	2×30		5800	
	23.Sep.2005	New UVES	2×30		8600	
14 594	26.Nov.2001	Archive	1800	40 000	3460	150
17 001	13.Dec.2001	Archive	4×1175	40 000	3460	110
17 147	26.Nov.2001	Archive	480	40 000	3460	140
18 802	28.Nov.2001	Archive	1500	35 000	3460	100
19 007	16.Oct.2005	New UVES	2×1200	35 000	3460	50
	16.Oct.2005	New UVES	2×500		5800	
	16.Oct.2005	New UVES	2×500		8600	
19 814	16.Oct.2005	New UVES	2×2400	35 000	3460	55
	16.Oct.2005	New UVES	2×1100		5800	
	16.Oct.2005	New UVES	2×1100		8600	
21 609	23.Sep.2005	New UVES	2×1800	35 000	3460	60
	23.Sep.2005	New UVES	2×800		5800	
	23.Sep.2005	New UVES	2×800		8600	
22 632	21.Sep.2005	New UVES	2×900	35 000	3460	60
	21.Sep.2005	New UVES	2×350		5800	
	21.Sep.2005	New UVES	2×350		8600	
24 030	08.Oct.2005	New UVES	2×1500	35 000	3460	75
	08.Oct.2005	New UVES	2×650		5800	
	08.Oct.2005	New UVES	2×650		8600	
24 316	22.Sep.2005	New UVES	2×1200	35 000	3460	70
	22.Sep.2005	New UVES	2×500		5800	
	22.Sep.2005	New UVES	2×500		8600	
31 188	26.Nov.2005	New UVES	2×700	35 000	3460	80
	26.Nov.2005	New UVES	2×300		5800	
	26.Nov.2005	New UVES	2×300		8600	
31 639	24.Sep.2005	New UVES	2×1200	35 000	3460	25
	24.Sep.2005	New UVES	2×500		5800	
	24.Sep.2005	New UVES	2×500		8600	
33 221	01.Dec.2001	Archive	4200	35 000	3460	145
	26.Dec.2001	Archive	4200		3460	
	27.Dec.2001	Archive	4200		3460	
33 582	10.Nov.2005	New UVES	2×900	35 000	3460	65
	10.Nov.2005	New UVES	2×350		5800	
	10.Nov.2005	New UVES	2×350		8600	
34 285	10.Apr.2000	Archive	4500	40 000	3460	100
	11.Apr.2000	Archive	3600	50 000	3460	
36 491	24.Dec.2005	New UVES	2×500	35 000	3460	40
	24.Dec.2005	New UVES	2×250		5800	
	24.Dec.2005	New UVES	2×250		8600	
36 640	08.Oct.2005	New UVES	2×150	35 000	3460	130
	08.Oct.2005	New UVES	2×30		5800	
	08.Oct.2005	New UVES	2×30		8600	
36 818	25.Nov.2001	Archive	5400	35 000	3460	75
36 849	25.Nov.2001	Archive	2×2100	35 000	3460	130

Table 2. continued.

HIP	Date of obs.	Type[1]	Exp. time (s)	R	λ_c (Å)	S/N^2 (final)
37 853	08.Apr.2001	UVES POP	2×60	80 000	3460	80
38 625	20.Dec.2005	New UVES	4×360	35 000	3460	60
	20.Dec.2005	New UVES	6×120		5800	
	20.Dec.2005	New UVES	2×120		8600	
42 592	20.Dec.2005	New UVES	2×900	35 000	3460	90
	20.Dec.2005	New UVES	2×350		5800	
	20.Dec.2005	New UVES	2×360		8600	
44 075	14.Apr.2001	UVES POP	200	80 000	3460	60
44 124	01.Feb.2005	Archive	3×1066	40 000	3460	105
	01.Feb.2005	Archive	3×800		5800	
45 554	24.Dec.2005	New UVES	2×3000	35 000	3460	45
	24.Dec.2005	New UVES	2×1400		5800	
	24.Dec.2005	New UVES	2×1400		8600	
48 152	29.Nov.2002	UVES POP	3×400	80 000	3460	115
50 139	05.Jan.2006	New UVES	2×400	35 000	3460	90
	05.Jan.2006	New UVES	2×130		5800	
	05.Jan.2006	New UVES	2×130		8600	
52 771	20.Mar.2005	Archive	3×1066	40 000	3460	40
53 070	05.Jan.2006	New UVES	600	35 000	3460	60
	05.Jan.2006	New UVES	2×200		8600	
55 022	10.Apr.2000	Archive	3×1800	40 000	3460	90
57 265	14.Jan.2006	New UVES	2×2100	35 000	3460	50
	14.Jan.2006	New UVES	2×900		5800	
	14.Jan.2006	New UVES	2×900		8600	
58 145	14.Jan.2006	New UVES	2×1800	35 000	3460	85
	14.Jan.2006	New UVES	2×800		5800	
	14.Jan.2006	New UVES	2×800		8600	
58 962	12.Jan.2002	Archive	2×4800	35 000	3460	70
59 490	12.Apr.2000	Archive	2×3600	40 000	3460	70
59 750	30.Jan.2006	New UVES	2×150	35 000	3460	100
	30.Jan.2006	New UVES	2×30		5800	
	30.Jan.2006	New UVES	2×30		8600	
60 632	28.Mar.2004	Archive	3×1066	40 000	3460	70
62 882	10.Apr.2000	Archive	2×1800	40 000	3460	155
63 559	19.Jan.2006	New UVES	2×300	35 000	3460	75
	19.Jan.2006	New UVES	1×200		5800	
	19.Jan.2006	New UVES	2×200		8600	
63 918	10.Apr.2000	Archive	2×3600	40 000	3460	100
64 426	08.Jun.2006	New UVES	3×450	35 000	3460	145
	08.Jun.2006	New UVES	4×150		5800	
	08.Jun.2006	New UVES	2×150		8600	
66 665	15.Jun.2006	New UVES	2×1000	35 000	3460	50
	15.Jun.2006	New UVES	2×400		5800	
	15.Jun.2006	New UVES	2×400		8600	
67 655	21.Feb.2002	Archive	2×900	35 000	3460	100
67 863	11.Apr.2001	Archive	3600	40 000	3460	145
70 681	09.Apr.2000	Archive	2×2700	50 000	3460	100
71 458	04.Feb.2002	Archive	5×250	40 000	3460	170
72 461	25.Jun.2006	New UVES	2×1800	40 000	3460	60
	25.Jun.2006	New UVES	2×800		5800	
	25.Jun.2006	New UVES	2×800		8600	
74 067	12.Jun.2006	New UVES	2×500	35 000	3460	100
	12.Jun.2006	New UVES	2×200		5800	
	12.Jun.2006	New UVES	2×200		8600	
74 079	12.Jun.2006	New UVES	2×400	35 000	3460	85
	12.Jun.2006	New UVES	2×150		5800	
	12.Jun.2006	New UVES	2×150		8600	
77 946	11.Jun.2006	New UVES	2×800	35 000	3460	65
	11.Jun.2006	New UVES	2×300		5800	
	11.Jun.2006	New UVES	2×300		8600	
80 003	12.Jun.2006	New UVES	2×2400	35 000	3460	30
	12.Jun.2006	New UVES	2×900		5800	
	12.Jun.2006	New UVES	2×900		8600	
80 837	04.Jun.2006	New UVES	4×300	35 000	3460	110
	04.Jun.2006	New UVES	4×100		5800	

Table 2. continued.

HIP	Date of obs.	Type[1]	Exp. time (s)	R	λ_c (Å)	S/N^2 (final)
	04.Jun.2006	New UVES	4×100		8600	
81 170	05.Aug.2003	Archive	3×1333	40 000	3460	45
85 963	04.Jun.2006	New UVES	2×400	35 000	3460	70
	04.Jun.2006	New UVES	2×150		5800	
	04.Jun.2006	New UVES	2×150		8600	
87 693	10.Apr.2000	Archive	2×3600	40 000	3460	70
88 010	07.Aug.2003	Archive	3×1333	40 000	3460	70
92 781	10.Apr.2000	Archive	2×1800	40 000	3460	100
94 449	12.Jun.2006	New UVES	2×1000	35 000	3460	90
	12.Jun.2006	New UVES	2×400		5800	
	12.Jun.2006	New UVES	2×400		8600	
98 020	11.Apr.2001	Archive	2700	50 000	3460	110
98 532	09.Apr.2000	Archive	2×900	50 000	3460	140
100 568	12.Jun.2006	New UVES	2×800	35 000	3460	120
	12.Jun.2006	New UVES	2×300		5800	
	12.Jun.2006	New UVES	2×300		8600	
100 792	25.Jun.2006	New UVES	2×700	35 000	3460	50
	25.Jun.2006	New UVES	2×300		5800	
	25.Jun.2006	New UVES	2×300		8600	
101 346	10.Apr.2000	Archive	2×1500	40 000	3460	85
103 498	04.Jun.2006	New UVES	2×600	35 000	3460	80
	04.Jun.2006	New UVES	2×200		5800	
	04.Jun.2006	New UVES	2×200		8600	
104 660	30.Jun.2006	New UVES	2×500	35 000	3460	40
	30.Jun.2006	New UVES	2×200		5800	
	30.Jun.2006	New UVES	2×200		8600	
105 858	07.Dec.2002	UVES POP	3×80	80 000	3460	400
105 888	18.Oct.2005	Archive	800	40 000	3460	65
106 447	25.Jun.2006	New UVES	2×3600	35 000	3460	45
	25.Jun.2006	New UVES	6×1100		5800	
	30.Jun.2006	New UVES	3600	35 000	3460	
	30.Jun.2006	New UVES	3×1100		8600	
107 975	30.Jun.2006	New UVES	2×150	35 000	3460	55
	30.Jun.2006	New UVES	2×10		5800	
	30.Jun.2006	New UVES	2×10		8600	
108 490	12.Jun.2006	New UVES	300	35 000	3460	90
	12.Jun.2006	New UVES	2×30		8600	
	09.Jul.2006	New UVES	300	35 000	3460	
	09.Jul.2006	New UVES	2×30		5800	
109 067	13.Oct.2005	New UVES	1500	35 000	3460	50
	13.Oct.2005	New UVES	2×650		5800	
109 558	29.May.2006	New UVES	1800	35 000	3460	55
	29.May.2006	New UVES	2×600		5800	
109 646	30.Jun.2006	New UVES	2×400	35 000	3460	105
	30.Jun.2006	New UVES	2×150		5800	
	30.Jun.2006	New UVES	2×150		8600	
112 229	30.Jun.2006	New UVES	400	35 000	3460	45
	30.Jun.2006	New UVES	2×150		8600	
114 271	17.Oct.2005	New UVES	1200	35 000	3460	120
	17.Oct.2005	New UVES	2×500		8600	
114 962	29.May.2006	New UVES	2×600	35 000	3460	100
	29.May.2006	New UVES	2×200		5800	
	29.May.2006	New UVES	2×200		8600	
115 167	11.Aug.2003	Archive	3×1066	40 000	3460	65
117 041	13.Oct.2005	New UVES	1800	35 000	3460	35
	13.Oct.2005	New UVES	2×800		5800	
G05-19	15.Oct.2005	New UVES	2700	35 000	3460	55
	15.Oct.2005	New UVES	3000	35 000	3460	
	15.Oct.2005	New UVES	2×1300		5800	
	15.Oct.2005	New UVES	2×1400		8600	
G05-40	08.Oct.2001	Archive	2×4800	35 000	3460	90
	22.Nov.2001	Archive	2×4800	35 000	3460	
G66-51	02.Jun.2006	New UVES	2×2400	35 000	3460	30
	02.Jun.2006	New UVES	2×900		5800	
	02.Jun.2006	New UVES	2×900		8600	

Table 2. continued.

HIP	Date of obs.	Type[1]	Exp. time (s)	R	λ_c (Å)	S/N[2] (final)
G166-37	02.Jun.2006	New UVES	3600	35 000	3460	25
	02.Jun.2006	New UVES	3×1100		5800	
	12.Jun.2006	New UVES	2×3600	35 000	3460	
	12.Jun.2006	New UVES	3×1100		5800	
	12.Jun.2006	New UVES	3×1100		8600	
G170-21	01.Jun.2006	New UVES	3600	35 000	3460	35
	01.Jun.2006	New UVES	3×1100		5800	
	02.Jun.2006	New UVES	3600	35 000	3460	
	02.Jun.2006	New UVES	3×1100		5800	
	02.Jun.2006	New UVES	2×1100		8600	
	12.Jun.2006	New UVES	3600	35 000	3460	
	12.Jun.2006	New UVES	3×1100		8600	

[1] Whether the spectra are from new observations, the ESO archive data, or the UVES POP library; [2] the S/N per pixel of the final combined spectrum in the Be region.

Table 3. Atmospheric parameters, as adopted from the literature, beryllium abundances as derived in this work, and lithium abundances, adopted from the literature when available or derived in this work when not. Details on the parameters and the abundances are given in the text. The reference papers of the atmospheric parameters and lithium abundances are also listed.

Star	$T_{\rm eff}$ Kelvin	log g Liter.	log g Paral.	ξ km s^{-1}	[Fe/H]	Ref.	log(Be/H) 3131	log(Be/H) average	A(Li)	Ref.
HIP 171	5275	4.10	4.30	1.05	−0.90	F00	−11.55	−11.51	≤0.80	(1)
HIP 3026	5950	3.90	4.10	1.40	−1.20	F00	−12.13	−12.11	2.42	(2)
HIP 7459	5909	4.46	4.59	1.23	−1.15	NS97	−11.90	−11.88	2.12	(3)
HIP 10140	5425	4.10	4.25	0.85	−1.00	F00	−11.68	−11.64	1.54	(2)
HIP 10449	5640	4.40	4.38	1.00	−0.80	F00	−11.31	−11.31	1.00	(4)
HIP 11952	6100	4.20	4.25	0.95	−1.60	F00	−12.28	−12.26	2.16	(2)
HIP 13366	5700	4.20	4.09	0.95	−0.70	F00	−11.07	−11.04	1.28	(3)
HIP 14086	5075	3.60	3.48	1.10	−0.60	F00	–	–	–	–
HIP 14594	5825	4.20	4.42	1.10	−2.00	F00	−12.63	−12.58	2.18	(2)
HIP 17001	5360	3.00	–	1.20	−2.35	GS88	≤−13.83	–	1.17	(2)
HIP 17147	5800	4.30	4.29	1.10	−0.80	F00	−11.20	−11.20	1.45	(3)
HIP 18802	5886	4.33	4.22	1.38	−0.85	NS97	−11.41	−11.41	1.89	(2)
HIP 19007	5150	4.50	4.74	1.20	−0.50	F00	–	–	–	–
HIP 19814	5378	4.43	–	0.84	−0.69	NS97	–	≤−11.64	0.98	(5)
HIP 21609	5200	3.80	4.55	1.55	−1.60	F00	–	–	1.43	(2)
HIP 22632	5825	4.30	4.41	1.35	−1.40	F00	−12.17	−12.14	2.17	(2)
HIP 24030	5700	4.20	4.26	1.11	−1.20	Pr00	−11.55	−11.53	2.08	(3)
HIP 24316	5725	4.40	4.45	1.30	−1.50	F00	−11.98	−11.96	2.00	(2)
HIP 31188	5750	4.10	4.28	1.65	−0.70	F00	−11.46	−11.46	1.95	(4)
HIP 31639	5300	4.30	4.55	0.60	−0.50	F00	−11.27	−11.15	≤0.50	(4)
HIP 33221	6097	4.09	4.00	1.86	−1.30	NS97	−11.67	−11.67	2.32	(3)
HIP 33582	5725	4.30	4.32	1.25	−0.50	F00	−11.09	−11.09	1.10	(4)
HIP 34285	5933	4.26	4.30	1.50	−0.90	NS97	−11.85	−11.85	2.22	(3)
HIP 36491	5800	4.40	4.39	1.10	−0.80	F00	−11.40	−11.40	1.70	(6)
HIP 36640	5830	3.64	–	0.70	−0.70	GS91	−11.44	−11.42	2.36	(3)
HIP 36818	5672	4.57	4.88	0.90	−0.83	NS97	–	≤−12.58	≤0.70	(3)
HIP 36849	5850	4.10	4.15	1.10	−0.70	F00	−11.35	−11.33	1.96	(3)
HIP 37853	5822	4.42	4.18	1.21	−0.78	Ed93	−11.16	−11.19	1.37	(3)
HIP 38625	5200	4.40	4.57	0.30	−0.70	F00	−11.42	–	≤0.16	(7)
HIP 42592	6025	4.10	4.02	1.20	−2.00	F00	−12.58	−12.58	2.12	(2)
HIP 44075	5900	4.20	4.11	1.25	−0.70	F00	−11.12	−11.12	2.06	(3)
HIP 44124	5750	3.60	–	0.10	−1.80	F00	−12.92	−12.86	1.96	(4)
HIP 45554	6021	4.44	3.96	1.34	−0.75	NS97	−11.45	−11.45	2.09	(3)
HIP 48152	6375	4.10	4.06	2.25	−2.00	F00	−12.67	−12.67	2.25	(2)
HIP 50139	5600	4.30	4.30	0.35	−0.70	F00	−11.28	−11.23	≤0.40	(4)
HIP 52771	5700	4.50	4.48	1.30	−1.80	F00	–	−12.55	2.16	(2)
HIP 53070	5900	4.20	4.27	1.45	−1.40	F00	−11.80	−11.80	2.21	(2)
HIP 55022	6450	4.20	4.05	1.80	−0.80	F00	–	≤−12.75	≤1.31	(2)
HIP 57265	5875	4.00	4.13	1.50	−1.00	F00	−11.90	−11.90	2.55	(5)
HIP 58145	5946	4.41	3.96	1.32	−1.04	NS97	−11.31	−11.31	1.95	(3)
HIP 58962	5831	4.36	–	1.30	−0.80	NS97	−11.68	−11.64	1.95	(3)
HIP 59490	6046	4.46	4.46	1.34	−1.26	NS97	−10.60	−10.58	2.51	(3)
HIP 59750	6200	4.40	4.26	1.10	−0.60	F00	–	≤−12.50	≤1.10	(3)
HIP 60632	6200	4.40	4.45	1.35	−1.50	F00	−12.10	−12.10	2.21	(2)
HIP 62882	5600	3.70	–	0.04	−1.10	F00	−11.20	−11.20	2.19	(8)
HIP 63559	5865	4.41	4.16	1.26	−0.93	NS97	–	–	2.14	(2)
HIP 63918	5720	4.14	3.91	1.49	−0.65	NS97	−10.95	−10.95	1.99	(3)
HIP 64426	5800	4.10	4.10	1.25	−0.70	F00	−11.31	−11.31	2.01	(3)
HIP 66665	5500	3.80	3.77	1.05	−0.80	F00	−11.61	−11.63	0.90	(4)
HIP 67655	5396	4.38	4.62	0.92	−0.93	NS97	−11.69	−11.50	≤1.25	(2)
HIP 67863	5686	4.40	4.42	1.13	−0.70	NS97	−10.95	−10.95	≤1.34	(2)
HIP 70681	5450	4.50	4.55	0.80	−1.10	F00	−11.12	−11.12	1.54	(3)
HIP 71458	5480	3.10	–	1.98	−2.10	McW95	≤−13.90	–	1.29	(2)
HIP 72461	5875	4.10	4.31	0.40	−2.30	F00	–	–	2.22	(2)
HIP 74067	5575	4.30	4.41	1.10	−0.80	F00	−11.36	−11.36	0.95	(4)
HIP 74079	5825	4.00	3.92	1.30	−0.70	F00	−11.28	−11.28	2.24	(2)
HIP 77946	6550	3.60	3.70	1.65	−0.90	F00	≤−12.95	≤−12.85	≤1.45	(6)
HIP 80003	5486	4.80	4.80	0.00	−0.87	SB02	−11.62	−11.62	1.25	(5)
HIP 80837	5800	4.10	4.07	1.15	−0.70	F00	−11.22	−11.20	1.53	(9)

Table 3. continued.

Star	T_{eff} Kelvin	log g Liter.	log g Paral.	ξ km s^{-1}	[Fe/H]	Ref.	log(Be/H) 3131	log(Be/H) average	A(Li)	Ref.
HIP 81170	5175	4.70	4.64	0.30	−1.10	F00	−11.53	−11.42	≤0.30	(10)
HIP 85963	6227	3.94	3.75	2.16	−0.71	Ed93	−11.78	−11.78	≤0.70	(4)
HIP 87693	6175	4.00	3.99	0.90	−2.00	F00	−12.77	−12.77	2.20	(2)
HIP 88010	5200	4.00	4.15	0.70	−1.40	F00	−12.40	−12.34	1.67	(2)
HIP 92781	5650	4.20	4.12	0.95	−0.60	F00	−11.14	−11.14	–	–
HIP 94449	5625	3.70	3.74	1.15	−1.20	F00	−11.50	−11.50	1.81	(6)
HIP 98020	5325	4.60	4.54	1.10	−1.60	F00	–	–	1.61	(2)
HIP 98532	5550	3.60	–	1.30	−1.10	F00	−11.43	−11.43	2.15	(3)
HIP 100568	5650	4.40	4.51	1.10	−1.00	F00	−11.98	−11.92	1.92	(2)
HIP 100792	5875	4.20	4.26	1.40	−1.10	F00	−11.97	−11.93	2.02	(2)
HIP 101346	6000	3.90	3.74	1.40	−0.50	F00	−11.52	−11.52	2.15	(9)
HIP 103498	5894	4.38	4.29	1.32	−1.03	Ed93	−11.36	−11.39	2.00	(11)
HIP 104660	5500	3.90	4.01	1.15	−0.80	F00	−11.41	−11.44	1.10	(2)
HIP 105858	6139	4.34	4.26	1.57	−0.67	Ed93	−11.32	−11.32	2.39	(3)
HIP 105888	5700	4.00	3.99	1.00	−0.60	F00	−11.13	−11.13	1.37	(6)
HIP 106447	6089	4.04	–	1.50	−2.48	SB02	−12.88	–	2.23	(5)
HIP 107975	6275	3.90	3.87	1.50	−0.50	F00	−12.25	−12.25	≤1.10	(9)
HIP 108490	6009	4.41	4.30	1.37	−0.72	Ed93	−11.34	−11.30	2.31	(3)
HIP 109067	5300	4.30	4.68	0.85	−0.80	F00	−11.39	−11.37	≤0.10	(4)
HIP 109558	6025	4.00	4.09	1.10	−1.50	F00	−12.30	−12.34	2.10	(2)
HIP 109646	5910	4.25	4.21	1.50	−0.64	Ed93	−11.38	−11.36	2.23	(3)
HIP 112229	5983	4.37	4.16	1.40	−0.65	Ed93	−11.21	−11.25	2.31	(3)
HIP 114271	6200	4.10	4.21	0.90	−1.70	F00	−12.44	−12.39	2.32	(2)
HIP 114962	5825	4.30	3.81	1.40	−1.40	F00	−12.40	−12.34	2.25	(2)
HIP 115167	6100	3.80	3.57	1.15	−1.50	F00	−12.45	−12.45	2.17	(2)
HIP 117041	5300	4.20	4.11	0.90	−0.80	F00	−11.34	−11.34	≤0.10	(4)
G05-19	5942	4.24	–	0.89	−1.10	SB02	−11.98	−12.01	2.26	(5)
G05-40	5863	4.24	–	1.48	−0.83	NS97	−11.15	−11.15	1.90	(3)
G66-51	5255	4.48	–	0.90	−1.00	Pr00	−11.47	−11.37	≤0.30	(4)
G166-37	5300	4.80	4.69	0.60	−1.20	F00	–	–	1.28	(5)
G170-21	5664	4.65	–	0.00	−1.45	SB02	−11.65	−11.58	1.91	(5)

(1) Takeda & Kawanomoto (2005); (2) Charbonnel & Primas (2005); (3) Chen et al. (2001); (4) this work; (5) Boesgaard et al. (2005); (6) Fulbright (2000); (7) Favata et al. (1996); (8) Ryan & Deliyannis (1995); (9) Romano et al. (1999); (10) Spite et al. (1994); (11) Gratton et al. (2000).

Table 6. The probabilities of each star of belonging to the thin disk, the thick disk, and the halo as calculated by Venn (2004), the kinematic classification[1] according to Gratton et al. (2003a,b), the average [α/Fe], and the orbital parameters: minimum radii (R_{min}), maximum radii (R_{max}), maximum distance from the plane (Z_{max}), eccentricity, and rotational velocity.

Star	Thin disk prob.	Thick disk prob.	Halo prob.	Gratton clas.[1]	[α/Fe]	R_{min}	R_{max}	Z_{max}	ecc.	V_{rot}
HIP 171	0.20	0.80	0.00	0	0.41	4.58	8.50	0.31	0.30	152.63
HIP 3026	0.00	0.00	1.00	1	0.30	0.19	10.72	7.62	0.97	−10.61
HIP 7459	0.00	0.00	1.00	1	0.17	0.67	16.87	8.34	0.92	−38.62
HIP 10140	0.00	0.90	0.10	0	0.29	4.29	8.97	0.61	0.35	147.98
HIP 10449	0.00	0.00	1.00	1	0.33	0.40	12.82	6.64	0.94	22.69
HIP 11952[2]	0.00	0.90	0.10	0	0.43	3.70	8.67	0.42	0.40	122.0
HIP 13366	0.00	0.70	0.30	0	0.31	3.35	8.85	1.65	0.45	120.06
HIP 14086	0.10	0.90	0.00	0	0.34	5.27	9.02	1.05	0.26	167.76
HIP 14594	0.00	0.10	0.90	0	0.41	2.34	12.24	1.52	0.68	102.15
HIP 17001	0.00	0.00	1.00	–	0.16	–	–	–	–	–
HIP 17147	0.00	0.90	0.10	0	0.33	3.74	9.93	0.52	0.45	140.82
HIP 18802	0.30	0.70	0.00	0	0.18	4.30	11.06	0.05	0.44	162.33
HIP 19007	0.90	0.10	0.00	2	0.21	7.95	10.97	0.11	0.16	236.72
HIP 19814[2]	0.00	0.00	1.00	1	0.05	0.58	31.41	10.39	0.96	28.00
HIP 21609	0.00	0.00	1.00	1	0.45	1.51	47.65	2.24	0.94	89.89
HIP 22632	0.00	0.90	0.10	0	0.36	3.48	8.87	0.24	0.44	128.43
HIP 24030	0.00	0.80	0.20	0	0.28	4.06	8.66	2.49	0.36	131.64
HIP 24316	0.00	0.00	1.00	1	0.37	2.65	15.78	4.71	0.71	−120.15
HIP 31188	0.00	0.90	0.10	0	0.13	6.98	8.68	1.42	0.11	191.26
HIP 31639	0.20	0.70	0.00	0	0.27	5.71	8.55	0.55	0.20	173.93
HIP 33221	0.00	0.70	0.30	0	0.28	6.67	8.88	3.43	0.14	175.82
HIP 33582	0.00	0.00	1.00	0	0.37	1.74	14.68	0.18	0.79	89.37
HIP 34285	0.00	0.00	1.00	1	0.05	0.63	25.25	2.14	0.95	−43.26
HIP 36491	0.00	0.80	0.20	0	0.30	2.60	8.71	0.04	0.54	103.85
HIP 36640	0.00	0.00	1.00	–	0.06	–	–	–	–	–
HIP 36818	0.00	0.00	1.00	1	0.04	0.66	14.63	1.73	0.91	−37.34
HIP 36849	0.00	0.90	0.10	0	0.26	3.69	9.27	0.78	0.43	134.34
HIP 37853[2]	0.00	0.00	1.00	0	0.28	3.96	11.00	0.38	0.47	141.60
HIP 38625	0.20	0.80	0.00	0	0.28	4.92	9.39	0.08	0.31	166.78
HIP 42592	0.00	0.00	1.00	1	0.30	2.92	21.49	3.08	0.76	−137.69
HIP 44075	0.00	0.80	0.20	0	0.34	3.95	8.75	1.74	0.38	134.02
HIP 44124	0.00	0.00	1.00	0	0.29	0.76	13.22	0.17	0.89	46.74
HIP 45554[2]	0.00	0.00	1.00	1	0.08	1.02	8.65	2.90	0.79	−0.62
HIP 48152	0.00	0.00	1.00	1	0.38	0.19	15.58	9.08	0.98	−12.26
HIP 50139	0.50	0.40	0.00	0	0.25	5.80	10.44	0.22	0.29	193.21
HIP 52771	0.00	0.00	1.00	1	0.45	2.89	12.65	1.75	0.63	−117.71
HIP 53070	0.00	0.60	0.40	0	0.44	2.01	8.58	0.18	0.62	85.88
HIP 55022	0.00	0.50	0.50	1	0.38	6.60	16.23	2.46	0.42	235.35
HIP 57265[2]	0.00	0.00	1.00	1	0.21	0.13	43.31	21.72	0.99	−6.00
HIP 58145[2]	0.00	0.90	0.10	0	0.24	4.87	8.55	1.37	0.27	143.00
HIP 58962[2]	0.00	0.00	1.00	1	0.06	0.56	8.54	2.75	0.88	21.00
HIP 59490	0.00	0.00	1.00	1	0.25	0.82	8.61	0.55	0.83	−44.47
HIP 59750	0.00	0.90	0.10	0	0.31	4.36	9.23	0.89	0.36	150.82
HIP 60632	0.00	0.00	1.00	1	0.41	0.21	10.92	6.77	0.96	11.03
HIP 62882	0.00	0.00	1.00	1	0.37	0.33	21.76	10.23	0.97	22.14
HIP 63559	0.00	0.00	1.00	1	0.11	0.38	9.00	5.19	0.92	−18.24
HIP 63918	0.00	0.00	1.00	1	0.21	1.67	9.70	0.07	0.71	−80.00
HIP 64426	0.00	0.90	0.10	0	0.29	4.58	9.52	1.35	0.35	155.72
HIP 66665[2]	0.00	0.20	0.80	0	0.36	3.28	12.57	2.19	0.59	123.00
HIP 67655	0.30	0.70	0.00	0	0.22	5.82	8.75	0.38	0.19	177.72
HIP 67863	0.00	0.00	1.00	1	0.22	0.59	9.01	6.24	0.88	−27.24
HIP 70681	0.00	0.90	0.10	0	0.31	6.14	8.50	1.35	0.16	178.04
HIP 71458	0.00	0.00	1.00	–	0.35	–	–	–	–	–
HIP 72461	0.00	0.60	0.40	0	0.44	2.83	10.82	0.46	0.59	119.11
HIP 74067	0.00	0.90	0.10	0	0.30	4.95	8.53	1.09	0.27	157.5
HIP 74079	0.90	0.10	0.00	0	0.27	7.99	9.41	0.25	0.08	222.97
HIP 77946	0.00	0.00	1.00	0	0.42	2.20	10.66	4.03	0.66	94.05
HIP 80003[2]	0.00	0.00	1.00	1	0.21	3.19	25.24	4.32	0.78	146.00
HIP 80837	0.00	0.00	1.00	1	0.32	0.70	9.70	5.24	0.87	−39.51
HIP 81170	0.00	0.00	1.00	0	0.36	1.51	9.28	6.03	0.72	52.21
HIP 85963[2]	0.80	0.20	0.00	2	0.15	6.93	8.55	0.05	0.11	185.90
HIP 87693[2]	0.00	0.00	1.00	1	0.44	4.42	8.89	0.45	0.34	−164.00

Table 6. continued.

Star	Thin disk prob.	Thick disk prob.	Halo prob.	Gratton clas.[1]	[α/Fe]	R_{min}	R_{max}	Z_{max}	ecc.	V_{rot}
HIP 88010	0.00	0.00	1.00	1	0.31	0.94	21.21	2.37	0.92	−56.94
HIP 92781	0.00	0.20	0.80	0	0.29	1.73	9.83	0.41	0.70	80.00
HIP 94449	0.00	0.00	1.00	1	0.38	1.92	11.42	1.41	0.71	−90.38
HIP 98020	0.00	0.20	0.80	0	0.27	2.67	11.29	1.81	0.62	111.38
HIP 98532	0.00	0.50	0.50	0	0.39	2.34	9.31	1.00	0.60	97.36
HIP 100568	0.00	0.00	1.00	1	0.20	0.45	10.59	1.87	0.92	−21.64
HIP 100792	0.00	0.00	1.00	1	0.24	0.97	8.88	0.34	0.80	−50.74
HIP 101346	0.60	0.40	0.00	0	0.16	5.76	9.53	0.06	0.25	187.90
HIP 103498[2]	0.10	0.80	0.00	0	0.30	4.94	8.75	0.33	0.28	151.00
HIP 104660	0.00	0.80	0.10	0	0.42	3.64	10.73	0.48	0.49	143.58
HIP 105858	0.90	0.10	0.00	0	0.09	8.43	12.69	0.12	0.20	249.80
HIP 105888[2]	0.00	0.70	0.30	0	0.35	2.47	8.54	0.56	0.55	99.52
HIP 106447[2]	0.00	0.00	1.00	1	0.42	0.89	23.80	2.15	0.93	44.00
HIP 107975	0.90	0.10	0.00	2	0.18	8.31	10.73	0.01	0.13	241.03
HIP 108490[2]	0.80	0.20	0.00	0	0.15	7.01	10.61	0.16	0.20	207.20
HIP 109067	0.00	0.00	1.00	1	0.31	0.15	8.57	6.14	0.97	4.57
HIP 109558	0.00	0.00	1.00	1	0.41	0.94	22.67	0.32	0.92	−55.85
HIP 109646[2]	0.20	0.70	0.00	0	0.10	8.39	11.73	1.36	0.17	235.40
HIP 112229[2]	0.50	0.40	0.00	0	0.12	7.56	11.14	0.76	0.19	219.20
HIP 114271	0.00	0.90	0.10	0	0.37	3.18	8.50	0.06	0.46	119.82
HIP 114962[2]	0.00	0.00	1.00	1	0.30	1.49	59.03	3.13	0.95	−109.00
HIP 115167[2]	0.00	0.00	1.00	1	0.38	4.19	38.98	3.17	0.81	−231.00
HIP 117041[2]	0.00	0.00	1.00	1	0.38	1.22	22.74	18.60	0.90	42.00
G05-19[2]	0.00	0.00	1.00	1	0.20	0.81	17.35	0.21	0.91	39.00
G05-40[2]	0.00	0.00	1.00	1	0.23	0.44	10.45	5.86	0.92	15.00
G66-51[2]	0.00	0.80	0.20	1	0.29	4.00	10.21	1.06	0.44	136.00
G166-37[2]	0.00	0.00	1.00	1	0.16	1.75	105.74	64.65	0.97	82.00
G170-21[2]	0.00	0.00	1.00	0	0.36	1.72	8.48	0.65	0.66	−88.00

[1] The following code is adopted: 0 for the accretion component, 1 for the dissipative component, and 2 for thin disk stars; [2] the orbital parameters for these stars were calculated in this work.

Appendix A: Detailed comparison

In this section we present a detailed comparison of our Be abundance results with previous results from the literature on a star-by-star basis. In most of the cases where differences in the abundances are seen, differences in the $\log g$ values can also be found. In these cases we are confident our results are robust since our $\log g$ values show excellent agreement with the ones derived using Hipparcos parallaxes.

HIP 171 (HD 224930)

The Be abundance of star HIP 171 was previously determined by Stephens et al. (1997), log(Be/H) = −11.02. The value we found, log(Be/H) = −11.55, is somewhat different. This difference is most probably a result of the different $\log g$ adopted; $\log g$ = 4.62 by Stephens et al. (1997) and $\log g$ = 4.10 by us.

HIP 11952 (HD 16031)

The Be abundance of HIP 11952 was previously determined by Gilmore et al. (1992). Adopting $\log g$ = 3.90 and [Fe/H] = −1.96 they found log(Be/H) = −12.37. Adopting $\log g$ = 4.20 and [Fe/H] = −1.60, we found log(Be/H) = −12.28, which shows a good agreement within the uncertainties, in spite of the different atmospheric parameters.

HIP 14594 (HD 19445)

The Be abundance of star HIP 14594 was previously determined by four papers. Rebolo et al. (1988) found an upper limit of log(Be/H) < −11.70, Ryan et al. (1990) found an upper limit of log(Be/H) < −12.30, Boesgaard & King (1993) found log(Be/H) = −12.14, and Boesgaard et al. (1999) found a range of values from log(Be/H)= −12.45 to −12.55. The value we derived, log(Be/H) = −12.63, is in good agreement with the lower limit of the range derived by Boesgaard et al. (1999).

HIP 17001 (CD−24 1782)

The Be abundance of star HIP 17001 was previously determined by García Pérez & Primas (2006) who found log(Be/H) = −13.45 in LTE and log(Be/H) = −13.54 in NLTE. We derived an upper limit of log(Be/H) < −13.83. The difference in the values is mainly due to the different $\log g$ adopted, 3.00 by us and 3.46 by García Pérez & Primas (2006).

HIP 17147 (HD 22879)

The Be abundance of HIP 17147 was previously determined by Beckman et al. (1989), log(Be/H) = −11.25, This value agrees well with the one found in this work, log(Be/H) = −11.20.

HIP 18802 (HD 25704)

The Be abundance of star HIP 18802 was previously determined by Molaro et al. (1997a), log(Be/H) = −11.61. In this work we found log(Be/H) = −11.41. The $\log g$ values, although similar, $\log g$ = 4.20 by Molaro et al. (1997a) and $\log g$ = 4.33 by us, account for a difference of ∼0.08 dex in the abundance, what would bring them to an agreement within the uncertainties.

HIP 24316 (HD 34328)

The Be abundance of HIP 24316 was previously determined by Gilmore et al. (1992), log(Be/H) = −11.90. This value agrees well with the value found in this work, log(Be/H) = −11.98.

HIP 37853 (HR 3018)

The Be abundance of HIP 37853 was previously determined by Gilmore et al. (1992), log(Be/H) = −11.20. This value agrees well with the one found in this work, log(Be/H) = −11.16.

HIP 42592 (HD 74000)

The Be abundance of star HIP 42592 was previously determined by Ryan et al. (1990), log(Be/H) < −12.20 and by Boesgaard et al. (1999), which found a range of values from log(Be/H) = −12.03 to −12.47. The value found in this work, log(Be/H) = −12.58, agrees with the lower limit of the range determined by Boesgaard et al. (1999), within the uncertainties. The small difference can be removed if we adopt the same $\log g$ used by Boesgaard et al., 0.16 dex higher than ours (increasing our abundance by ∼0.08 dex).

HIP 44075 (HD 76932)

The Be abundance of star HIP 44075 was determined by a number of papers in literature. Molaro & Beckman (1984) found an upper limit of log(Be/H) < −11.52, Beckman et al. (1989) found log(Be/H) = −11.69, both Gilmore et al. (1992) and Ryan et al. (1992) found log(Be/H) = −11.30, Boesgaard & King (1993) found log(Be/H) = −11.04, Garcia Lopez et al. (1995b) found log(Be/H) = −11.36 (in NLTE), Thorburn & Hobbs (1996) found log(Be/H) = −11.45, Molaro et al. (1997a) found −11.21, and Boesgaard et al. (1999) found a range of values from log(Be/H)= −11.17 to −11.24. The value we found, log(Be/H) = −11.12, is in the upper range of the values listed above and in good agreement with Boesgaard et al. (1999).

HIP 48152 (HD 84937)

For star HIP 48152, Ryan et al. (1992) found log(Be/H) < −12.85, Boesgaard & King (1993) found log(Be/H) = −12.85, Thorburn & Hobbs (1996) found log(Be/H) < −12.95, and Boesgaard et al. (1999), from log(Be/H)= −12.83 to −12.94. The value we derived is log(Be/H) = −12.67. Reducing our $\log g$ by 0.20 dex to match the one adopted by Boesgaard et al. (1999), for example, would reduce our abundance by ∼0.11 dex, resulting in an agreement within the uncertainties.

HIP 53070 (HD 94028)

For HIP 53070, Boesgaard & King (1993) found log(Be/H) = −11.56, Garcia Lopez et al. (1995b) found log(Be/H) = −11.66 (in NLTE), Thorburn & Hobbs (1996) found log(Be/H) = −11.65, and Boesgaard et al. (1999) found a range of values from log(Be/H)= −11.51 to −11.55. The value we derived is log(Be/H) = −11.80. Once again, a change in the adopted $\log g$ would bring the abundances to a better agreement.

HIP 55022 (HD 97916)

For HIP 55022, Boesgaard (2007) found log(Be/H) < −13.30 while we derived log(Be/H) < = −12.75.

HIP 59750 (HD 106516)

For HIP 59750, Molaro et al. (1997a) found log(Be/H) < −12.76 and Stephens et al. (1997) found log(Be/H) < −12.61. The upper-limit we derived is log(Be/H) < −12.50, agrees with the previous results within the uncertainties.

HIP 64426 (HD 114762)

For HIP 64426, Stephens et al. (1997) found log(Be/H) = −11.05, Boesgaard & King (1993) found log(Be/H) = −11.14, Santos et al. (2002) found log(Be/H) = −11.03, and Santos et al. (2004) found log(Be/H) = −11.18. The value we derived is log(Be/H) = −11.31. The difference is again related to the different choice of log g values.

HIP 71458 (HD 128279)

For HIP 71458, Molaro et al. (1997a) found log(Be/H) = −12.75 and by García Pérez & Primas (2006) found log(Be/H) < −14.01, in LTE, and log(Be/H) = −13.94 in NLTE. We derived an upper limit of log(Be/H) < −13.90.

HIP 74079 (HD 134169)

The Be abundance of HIP 74079 was previously determined by five papers. Gilmore et al. (1992) and Ryan et al. (1992) both found log(Be/H) = −11.35, Boesgaard & King (1993) found log(Be/H) = −11.29, Garcia Lopez et al. (1995b) found log(Be/H) = −11.23 (in NLTE), and Boesgaard et al. (1999) found a range of values from log(Be/H) = −11.32 to log(Be/H) = −11.40. All these values agree with ours, log(Be/H) = −11.28, within the uncertainties.

HIP 80837 (HD 148816)

The Be abundance of HIP 80837 was previously determined by Stephens et al. (1997), log(Be/H) = −11.07 and by Boesgaard & King (1993), log(Be/H) = −11.10. Both values are consistent with ours, log(Be/H) = −11.22, within the uncertainties.

HIP 87693 (BD+20 3603)

The Be abundance of star HIP 87693 was previously determined by Boesgaard et al. (1999) who found a range of values from log(Be/H) = −12.40 to log(Be/H) = −12.62. Our value, log(Be/H) = −12.77, is again consistent, within the uncertainties, with the lower limit of the range found by Boesgaard et al. (1999). The difference in the adopted log g values, 4.33 or 4.27 by Boesgaard et al. and 4.00 by us, seems to be the main reason for the different abundances.

HIP 98532 (HD 189558)

The Be abundance of star HIP 98532 was previously determined by Rebolo et al. (1988) who found log(Be/H) = −11.70 and by Boesgaard & King (1993) who found log(Be/H) = −10.99. Both papers claim higher uncertainties for this star when compared with the other stars of the sample. We determined a value of log(Be/H) = −11.43, which is intermediate between the two previous determinations.

HIP 100792 (HD 194598)

The Be abundance of star HIP 100792 was previously determined by three papers. Rebolo et al. (1988) found log(Be/H) = −11.70, Thorburn & Hobbs (1996) found log(Be/H) = −11.95, and Boesgaard et al. (1999) found a range of values from log(Be/H)= −11.73 to −11.88. The value determined in this work is log(Be/H) = −11.97. Our result agrees very well with the one from Thorburn & Hobbs (1996) although they adopt a smaller log g, 4.00, when compared to ours, log g = 4.20. Within the uncertainties, our result agrees with the lower limit of the range of values found by Boesgaard et al. (1999).

HIP 101346 (HD 195633)

The Be abundance of star HIP 101346 was previously determined in three papers. Boesgaard & King (1993) found log(Be/H) = −11.21, Stephens et al. (1997) found log(Be/H) = −11.29, and Boesgaard & Novicki (2006) found log(Be/H)= −11.34. Our value is somewhat smaller than these, log(Be/H) = −11.52. The parameter controlling most of this difference seems to be the metallicity. We adopt [Fe/H] = −0.50, while Boesgaard & King (1993) adopt [Fe/H] = −1.07, Stephens et al. (1997) [Fe/H] = −1.00, and Boesgaard & Novicki (2006) [Fe/H] = −0.88. Adopting the value of Boesgaard & Novicki (2006), for example, would increase our result by 0.08 dex, bringing the values to agree within the uncertainties.

HIP 104660 (HD 201889)

The Be abundance of star HIP 104660 was previously determined by Boesgaard & King (1993), log(Be/H) = −11.43, and by Boesgaard et al. (1999) which found a range of values from log(Be/H)= −11.30 to −11.38. Our value, log(Be/H) = −11.41, is in excellent agreement with these.

HIP 105858 (HR 8181)

The Be abundance of HIP 105858 was previously determined by Gilmore et al. (1992). A value of log(Be/H) = −11.40 was found, in excellent agreement with ours, log(Be/H) = −11.32.

HIP 107975 (HD 207978)

The Be abundance of star HIP 107975 was previously determined by Stephens et al. (1997), which found an upper limit of log(Be/H) < −12.38. Our analysis provides a detection mainly based on line 3131 Å, log(Be/H) = −12.25.

HIP 108490 (HD 208906)

The Be abundance of star HIP 108490 was previously determined in three papers. Boesgaard & King (1993) found log(Be/H) = −11.10, Stephens et al. (1997) found log(Be/H) = −11.19, and Boesgaard et al. (2004) found log(Be/H) = −11.30. This last value is in excellent agreement with our own, log(Be/H) = −11.34. The difference with Boesgaard & King (1993) can be explained by the smaller log g adopted by them, log g = 4.25,

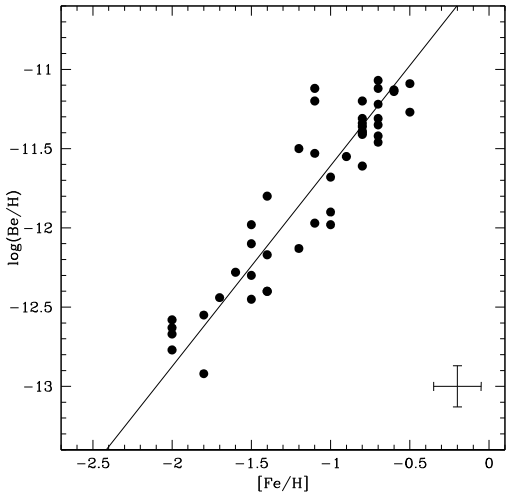

Fig. B.1. Diagram of [Fe/H] vs. log(Be/H) for the stars analyzed by Fulbright (2000). Only detections are shown. An example of error bar is shown in the lower right corner.

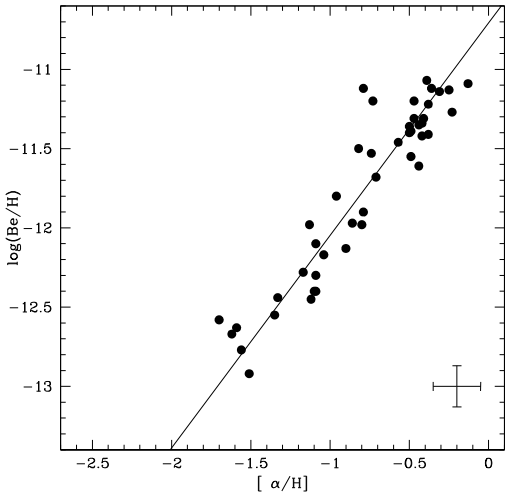

Fig. B.2. Diagram of [α/H] vs. log(Be/H) for the stars analyzed by Fulbright (2000). Only detections are shown. An example of error bar is shown in the lower right corner.

when compared with the one adopted in this work, $\log g = 4.41$ (and also by Boesgaard et al. 2004).

HIP 109558 (BD+17 4708)

The Be abundance of star HIP 109558 was previously determined by Boesgaard et al. (1999), who found a range of values from log(Be/H)= −12.28 to −12.42. Our result, log(Be/H) = −12.30, is in excellent agreement with this range.

HIP 114271 (HD 218502)

The Be abundance of HIP 114271 was previously determined by Molaro et al. (1997a), log(Be/H) = −12.56. Our result, log(Be/H) = −12.44, agrees with it within the uncertainties.

HIP 114962 (HD 219617)

For HIP 114962, Rebolo et al. (1988) found log(Be/H) < −11.60, Molaro et al. (1997a) found log(Be/H) = −12.56, and Boesgaard et al. (1999) found a range from log(Be/H) = −12.09 to −12.15. Our value, log(Be/H) = −12.40, is closer to the value found by Molaro et al. (1997a) than to the one by Boesgaard et al. (1999) although our parameters are very different from the former and similar to the latter.

Appendix B: F00 subsample

In this appendix we show plots of the relations between log(Be/H) and [Fe/H] (Fig. B.1) and between log(Be/H) and [α/H] (Fig. B.2) for the stars of the F00 subsample. The fits are statistically identical to the ones obtained with the whole clean sample.

Appendix C: Accretion and Dissipative Components

In this appendix we divide our sample in an "accretion" and a "dissipative" component according to the prescriptions of Gratton et al. (2003a,b).

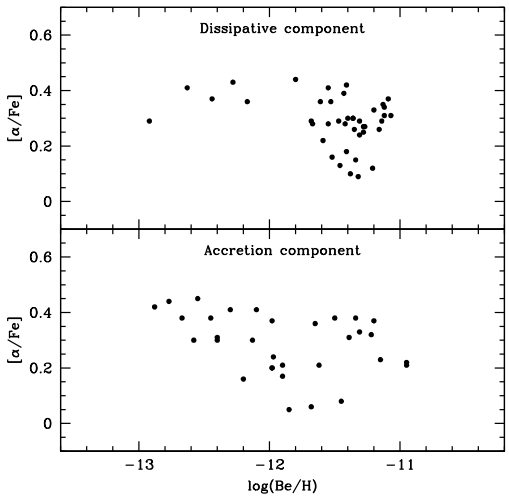

Fig. C.1. Diagram of [α/Fe] vs. log(Be/H). The dissipative component stars are shown in the *upper panel* while the accretion component stars are shown in the *lower panel*. The dissipative stars diagram is characterized by a large scatter while the accretion stars diagram clearly divides in two sequences.

The purpose is to test whether the same characteristics of our sample would be obtained with this different classification. The division of the stars according to this classification is also listed in Table 6. Some of the stars classified as thin disk stars by Venn et al. (2004) are classified as stars of the dissipative component by the criteria of Gratton et al. (2003a,b). In the clean sample we have 34 stars classified as accretion component and 39 as dissipative component. In Figs. C.1, C.2, C.3, and C.4, we show how these components behave in each of the plots presented before for the halo and thick disk components. Therefore, these should be directly compared with Figs. 17, 19, 20. As it can be seen, the overlap is really high and the conclusions obtained are the same.

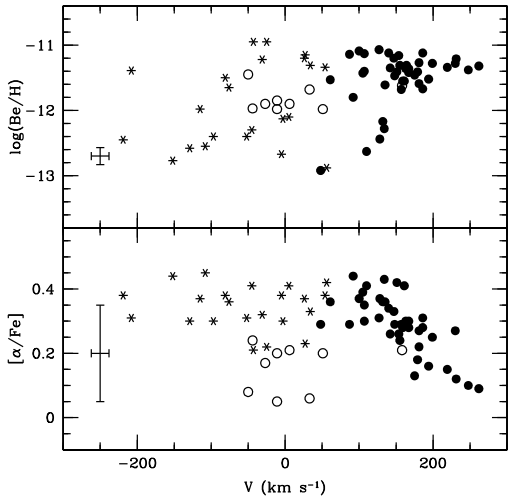

Fig. C.2. Diagram of et al. log(Be/H) vs. the V, the component of the space velocity of the star in the direction of the disk rotation. The dissipative component stars are shown as filled circles, accretion stars are shown as starred symbols, and the subgroup of accretion stars as open circles. A typical error of ±12 Km s^{-1} in V was adopted (see Gratton et al. 2003b).

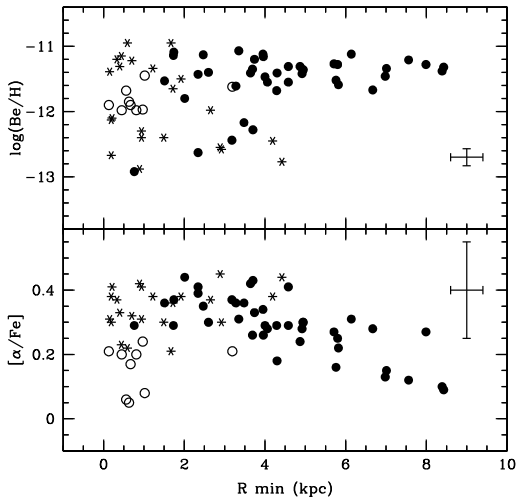

Fig. C.3. Diagram of log(Be/H) vs. $R_{\rm min}$, the perigalactic distance of stellar orbit. The dissipative stars are shown as filled circles, accretion stars are shown as starred symbols, and the subgroup of accretion stars as open circles. A typical error of ±0.40 Kpc in $R_{\rm min}$ was adopted (see Gratton et al. 2003b).

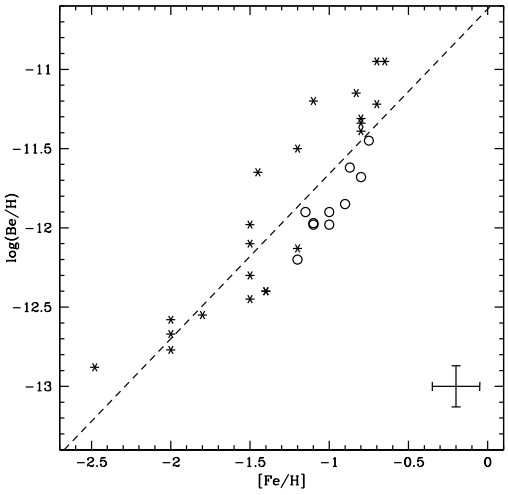

Fig. C.4. Diagram of log(Be/H) vs. [Fe/H] where only the accretion stars are shown. The subgroup of stars with low alpha is shown as open circles, the remaining accretion stars are shown as starred symbols. The linear fit for all the accretion stars is shown to guide the eye.